JGR Atmospheres

RESEARCH ARTICLE
10.1029/2024JD041170

The Abundance and Sources of Ice Nucleating Particles Within Alaskan Ice Fog

Emily Lill[1], Emily J. Costa[2], Kevin Barry[1], Jessica A. Mirrielees[2], Monica Mashkevich[2], Judy Wu[2], Andrew L. Holen[2], Meeta Cesler-Maloney[3], Paul J. DeMott[1], Russell Perkins[1], Thomas Hill[1], Amy Sullivan[1], Ezra Levin[4], William R. Simpson[3], Jingqiu Mao[3], Brice Temime-Roussel[5], Barbara D'Anna[5], Kathy S. Law[6], Andrew P. Ault[2], Carl Schmitt[7], Kerri A. Pratt[2,8], Emily V. Fischer[1], and Jessie Creamean[1]

[1]Department of Atmospheric Science, Colorado State University, Fort Collins, CO, USA, [2]Department of Chemistry, University of Michigan, Ann Arbor, MI, USA, [3]Department of Chemistry and Biochemistry and Geophysical Institute, University of Alaska Fairbanks, Fairbanks, AK, USA, [4]Handix Scientific, Fort Collins, CO, USA, [5]Aix Marseille University, CNRS, LCE, Marseille, France, [6]Sorbonne Université, UVSQ, CNRS, LATMOS-IPSL, Paris, France, [7]Alaska Climate Research Center, Geophysical Institute, University of Alaska Fairbanks, Fairbanks, AK, USA, [8]Department of Earth & Environmental Sciences, University of Michigan, Ann Arbor, MI, USA

Key Points:

- Fairbanks had higher wintertime ice nucleating particle (INP) concentrations than other high-latitude locations
- INP concentrations in Fairbanks decreased during the ice fog period, indicating that INPs were activated into the fog
- INP composition in Fairbanks was dominated by heat-labile INPs

Supporting Information:

Supporting Information may be found in the online version of this article.

Correspondence to:

E. Lill,
emily.lill@colostate.edu

Citation:

Lill, E., Costa, E. J., Barry, K., Mirrielees, J. A., Mashkevich, M., Wu, J., et al. (2024). The abundance and sources of ice nucleating particles within Alaskan ice fog. *Journal of Geophysical Research: Atmospheres*, *129*, e2024JD041170. https://doi.org/10.1029/2024JD041170

Received 19 MAR 2024
Accepted 1 AUG 2024

Abstract The Alaskan Layered Pollution and Chemical Analysis (ALPACA) field campaign included deployment of a suite of atmospheric measurements in January–February 2022 with the goal of better understanding atmospheric processes and pollution under cold and dark conditions in Fairbanks, Alaska. We report on measurements of particle composition, particle size, ice nucleating particle (INP) composition, and INP size during an ice fog period (29 January–3 February). During this period, coarse particulate matter (PM_{10}) concentrations increased by 150% in association with a decrease in air temperature, a stronger temperature inversion, and relatively stagnant conditions. Results also show a 18%–78% decrease in INPs during the ice fog period, indicating that particles had activated into the ice fog via nucleation. Peroxide and heat treatments performed on INPs indicated that, on average, the largest contributions to the INP population were heat-labile (potentially biological, 63%), organic (31%), then inorganic (likely dust, 6%). Measurements of levoglucosan and bulk and single-particle composition corroborate the presence of dust and aerosols from combustion sources. Heat-labile and organic INPs decreased during the peak period of the ice fog, indicating those were preferentially activated, while inorganic INPs increased, suggesting they remained as interstitial INPs. In general, INP concentrations were unexpectedly high in Fairbanks compared to other locations in the Arctic during winter. The fact that these INPs likely facilitated ice fog formation in Fairbanks has implications for other high latitude locations subject to the hazards associated with ice fog.

Plain Language Summary The Alaskan Layered Pollution and Chemical Analysis field campaign occurred January–February 2022 with the goal of better understanding the atmosphere and atmospheric pollution during the winter in Fairbanks, Alaska. We studied a rare subset of atmospheric particles called ice nucleating particles which facilitate the formation of ice fog by allowing water to freeze at temperatures above −38°C. During our study, there was an ice fog event that coincided with a pollution event. During this event, there was a significant increase in coarse particulate matter associated with a decrease in temperature and calm winds. Ice nucleating particle concentration in the air decreased during the ice fog event indicating that the INPs had activated into the ice fog and were not able to be captured. We determined that most INPs were heat-labile (potentially biological), followed by organic. Very few INPs were inorganic. Inorganic INPs increased during the ice fog period while heat-labile and organic INPs decreased indicating that they were being selectively activated into the fog. Overall, INP concentrations in Fairbanks were quite high compared to other Arctic locations and carries implications for ice fog formation in other high-latitude locations.

1. Introduction

Air pollution is an emerging issue for the Arctic with major contributions from both local and remote sources (Law & Stohl, 2007). The Arctic is often impacted by pollutants transported from North America, Asia, and Europe, specifically in the winter during the so-called Arctic haze (Law et al., 2014). In the summertime, wildfire smoke from both local and long-range sources can negatively impact Arctic air quality (Simpson et al., 2011; Woo et al., 2020). Industrial development is expected to increase in the Arctic due to warming temperatures, creating

opportunities for economic growth and a growing population (Larsen & Fondahl, 2015). Additionally, warming temperatures are predicted to lead to an increase in biogenic volatile organic compound (VOC) emissions (Kramshøj et al., 2016) and emissions from activities such as gas flaring due to the projected increased industrial development (Li et al., 2016). These conditions are likely to lead to worsening air quality (Law et al., 2017). In the winter, strong inversions can trap and lead to the accumulation of pollution (Cesler-Maloney et al., 2022; Schmale et al., 2018).

Air pollution in the Arctic is often concentrated by both topography and meteorology. In the winter, the Arctic experiences a lack of solar heating due to few hours of daylight coupled with a high surface albedo from the ubiquitous snowpack (Joyce et al., 2014). The minimal solar heating suppresses vertical convective mixing, which can lead to strong surface-based inversions (Wendler & Jayaweera, 1972). These surface-based inversions occur quite frequently: about 50% of the time from November to March in Fairbanks, Alaska, a subarctic city (Cesler-Maloney et al., 2022; Malingowski et al., 2014; Tran & Mölders, 2011). Additionally, Fairbanks is surrounded by hills, which shelter the region from winds (Willis & Grice, 1977). The combination of a strong inversion and weak winds create an environment with little dispersion, and pollutants can accumulate.

In the Arctic, ice fog formation is often linked to high levels of air pollution. When temperatures fall below −15°C, high levels of pollution can lead to the formation of ice fog, which can worsen visibility issues for transportation (Gultepe et al., 2017). Those living in communities affected by ice fog often experience aviation hazards due to poor visibility and aircraft icing (Gultepe et al., 2014). This is a major hindrance for communities that do not have access to highways as they depend on air travel for essential services and supplies. Ice fogs are also often indicative of extreme pollution events because of both non-activated aerosols and the ice fog itself (Robinson et al., 1957). Fairbanks is a unique urban environment that experiences conditions which are crucial for ice fog formation.

Low visibility due to high air pollution levels and ice fog formation can be routine in certain seasons in Fairbanks. Fairbanks, along with the larger Fairbanks-North Star Borough, routinely experiences wintertime $PM_{2.5}$ levels $>50\ \mu g\ m^{-3}$ (Schmale et al., 2018). This is due to increased energy usage in the winter that relies on coal, gasoline, fuel oil, and residential burning (Bowling, 1986). A portion of the increased wintertime energy needs is supplied by the four power plants located in the 32 square mile area of Fairbanks. The increased energy needs also result in increased residential heating, typically in the form of biomass burning of wood or fuel oil (Nicholls et al., 2010). Local emissions in Fairbanks are often trapped by low temperatures and steep surface-based inversions (Tran & Mölders, 2011). The power plants, automobiles, and the Chena River, which runs through downtown Fairbanks, provide sources of water vapor in the winter. Inversions with sufficient water vapor can also lead to ice fog which can reduce visibility down to 200 m (Schmitt et al., 2013).

The formation processes of ice fog are not well known. This is in part due to a limited understanding of the sources and characteristics of ice nucleating particles (INPs) and cloud condensation nuclei (CCN). Ice formation in fogs can happen through a variety of microphysical pathways, both homogeneous and heterogeneous. Homogeneous ice formation occurs at temperatures below about −38°C, and requires the presence of liquid water either through the cooling of an existing droplet or the condensation of supersaturated water vapor onto a CCN (Benson, 1970). Heterogeneous ice formation involves an INP, which are rare, and this pathway can be split into immersion / condensation, deposition, and contact freezing mechanisms (Gultepe et al., 2014, 2017; Huffman & Ohtake, 1971). Immersion freezing occurs when an INP is incorporated into a liquid droplet, either by acting as a CCN or being scavenged by a liquid droplet, and subsequently activating to freeze the droplet, generally as temperature decreases. Condensation freezing is often considered a subset of immersion freezing, requiring that freezing occurs concurrently with liquid water uptake. Deposition regime nucleation, by contrast, does not require the presence of water supersaturation that would lead to formation of liquid droplets; instead, it yields ice formation at water subsaturated conditions with temperatures below about −38°C. The exact pathway of freezing in this regime is unclear, and has been postulated to be freezing via deposition of ice on an aerosol surface, or condensation of liquid water in small pores within an aerosol that subsequently freeze, with strong evidence for the latter occurring in at least some cases (David et al., 2019). Contact nucleation occurs when an INP collides with a liquid droplet and immediately leads to freezing. These processes are crucial for ice fog formation, although the cumulative impact of INPs is poorly understood (Kanji et al., 2017). Crystals in an ice fog have been shown to form via immersion freezing, as well as, to a lesser degree, deposition freezing (Gultepe et al., 2017; Huffman & Ohtake, 1971).

Only a few studies from the 1960 and 1970s examined sources of INPs in ice fog, making ice fog significantly understudied compared to other ice cloud types and leaving major knowledge gaps in our understanding of how ice fog forms (Kikuchi, 1971a, 1971b, 1972; Kumai, 1964, 1966; Radke et al., 1976). Kumai (1964) measured ice crystal residuals and showed that at −39°C, the concentration of ice fog crystals in Fairbanks was 155 crystals/cm^3, and that they were likely from oil or coal burning sources. Kumai (1966) also measured ice fog crystal residuals in Fairbanks and reported ice fog crystal concentrations at various ice crystal diameters at −39°C. The largest concentration of ice fog crystals were observed at the following sizes: 5(32 crystals cm^{-3}), 3(28 crystals cm^{-3}), and 7 μm (26 crystals cm^{-3}). Kumai (1966) also reported that the residual nuclei were both organic and inorganic particles from coal, fuel oil, and gasoline combustion. Radke et al. (1976) measured interstitial INPs in an ice fog in Barrow (Utqiaġvik), Alaska and found the average INP concentration to be 0.15 INPs/L at −20°C. Kikuchi (1971a, 1971b, 1972) reported concentration measurements of CCN, INPs, and ice crystals in Antarctica and concluded that ice fog is likely the result of frozen water droplets, during a time when it was speculated that INPs were a result of meteor showers.

The effectiveness of INPs from pollution is debated, with studies reporting conflicting results. Generally, aerosol sources including sea spray, mineral dust, black carbon, and biologically-derived particles have been shown to contain small fractions of INPs, with efficiencies varying greatly between sources (Conen et al., 2011; DeMott et al., 2018; Hoose & Möhler, 2012; Petters et al., 2009). Pollution aerosols from combustion have been shown to be poor INPs compared to dust or biological particles (Bi et al., 2019; Levin et al., 2019). However, it has been shown that anthropogenic organic aerosols can be efficient INPs at temperatures below −30°C, as well as coal fly ash particles at temperatures below −15°C (Kanji et al., 2017; Murray et al., 2012; Tian et al., 2022). Some studies show that heavy pollution has no effect on INP concentrations. For example, Chen et al., 2018 showed that there was no correlation between INP concentration and $PM_{2.5}$ or black carbon mass concentration in Beijing, China even when $PM_{2.5}$ exceeded hundreds of μg m^{-3} Zhang et al. (2022) showed that during a dust event in Beijing, INP number concentrations increased from a background concentration of 10^{-1} to 10 L^{-1} to up to 160 L^{-1} at −30°C. They also showed that increases in black carbon did not have an effect on INP number concentrations. Borys (1989) showed that Arctic haze aerosols have 10–1,000 times lower ice nucleation rates than unpolluted Arctic air. Creamean et al. (2018) demonstrated that local springtime pollution did not impact INP concentrations at an Arctic oilfield location. In contrast, some studies show that pollution aerosols can serve as effective INPs. For example, Zhao et al. (2019) used 11-year continuous satellite observations from multiple satellites and cloud-resolving model simulations in East Asia and determined that polluted continental aerosols, excluding smoke and dust aerosols, contained a large fraction of INPs. An interannual and intraseasonal study at the Jungfraujoch research station, located in the Swiss Alps, found that polluted air masses from the Po valley and industrial regions of France had INP concentrations >100 L^{-1} compared to background conditions of 1–10 L^{-1} at −31 ± 0.4°C (Lacher et al., 2018). Schrod et al. (2020) found a moderate but significant correlation in PM_{10} and INP concentrations throughout the temperature spectrum at the Taunus Observatory (located ∼20 km NW of Frankfurt, Germany).

Here, we investigate the aerosol properties associated with an ice fog episode that occurred in Fairbanks from 29 January to 3 February 2022 during the Alaskan Layered Pollution And Chemical Analysis (ALPACA) study. To our knowledge, this is the first-time ice fog INP measurements have been made since the 1970s. We present total and size-resolved INP concentration data throughout the course of the event, in addition to days prior to and after the ice fog. We also utilize bulk aerosol mass and number concentrations, speciated metal mass concentrations, and single-particle composition data to better understand the general aerosol population sources. This is the first time a study has evaluated the sources and roles of INPs in ice fog formation in Fairbanks.

2. Data and Methods

2.1. ALPACA Overview

The ALPACA study occurred from 17 January 2022–25 February 2022 with the goal of better understanding pollution under cold and dark conditions (Simpson et al., 2019, 2024). Fairbanks, Alaska (64.8401°N, 147.7200°W) is a city with a population of 32,515 located within the Fairbanks-North Star Borough, which has a total population of 95,655, in the interior of Alaska. While Fairbanks itself is not technically within the Arctic circle, it has a subarctic climate subjected to conditions similar to that of the Arctic and may be representative of

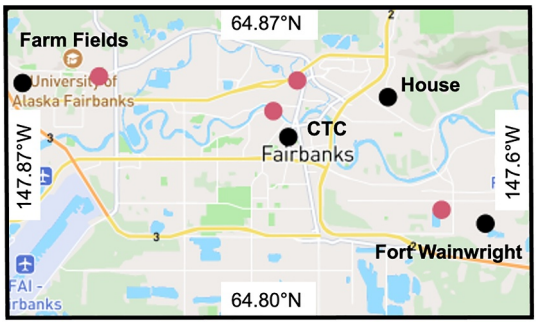

Figure 1. Map of Fairbanks, Alaska with study locations marked by black points and labeled. Power plants are marked by pink points.

conditions in Arctic communities. During this campaign, there were multiple field sites located throughout the Fairbanks-North Star Borough (Figure 1).

Measurements presented in our study were taken at the University of Alaska Fairbanks (UAF) Community Technical College (CTC) site (64.841°N, 147.727°W, 135 m AMSL) located in downtown Fairbanks. Instruments were housed within or located outside of two laboratory trailers at CTC. The ALPACA study also supported outdoor measurements at the University of Alaska Farm Field site and indoor measurements at a house in a residential community (these results are not discussed herein; see Simpson et al., 2024 for more details). Supplementary data used in our study were collected at Fort Wainwright. Gas, aerosol, and meteorological measurements were made at all of these sites. During the ALPACA study, there was one major pollution event that coincided with an ice fog event.

2.2. Measurement Techniques

2.2.1. Bulk Aerosol Mass and Metal Concentrations

The HORIBA, Ltd. PX-375 continuous particle mass and elemental speciation monitor was used to measure PM_{10} mass concentrations (μg m^{-3}) and concentrations of various metals (ng m^{-3}) (Creamean & Neiman et al., 2016). The PX-375 had a flow rate of 16.7 L min^{-1} through an EPA louvered PM_{10} inlet. Each sample consisted of 30 min of ambient collection. Particles were deposited on a 100 mm diameter spot on a Teflon™ PTFE fabric filter tape for beta-ray attenuation analysis for total PM_{10} mass concentrations, followed by energy dispersive x-ray fluorescence (EDXRF) analysis for concentrations of titanium, vanadium, chromium, manganese, iron, nickel, copper, zinc, arsenic, lead, aluminum, silicon, sulfur, potassium, and calcium. Lower detection limits are defined in Creamean and Neiman et al. (2016).

2.2.2. Particle Number Concentrations

Particle number concentration was monitored with a commercial optical particle counter (model OPC 1.109, Grimm Aerosol Technik) at a time resolution of 1 min. The OPC 1.109 classifies individual particles by optical diameter within 31 channels ranging from 0.25 to 32 μm, based on the intensity of light scattered by particles illuminated by a laser diode (655 nm, P_{max} = 40 mW) (Burkart et al., 2010; Heim et al., 2008). As the instrument is factory-calibrated with polystyrene latex (PSL) particles of controlled spherical shape and known refractive index (RI = 1.56 for PSL), and these parameters for complex ambient particles are not known, the size distribution measurements are expressed as optical latex equivalent diameters. Ambient air was drawn at 3.5 m above ground level into the OPC at a volume flow rate of 1.2 L min^{-1} through a short length (≈1.5 m) of ¼" o. d. Vertical anti-static tube extending outside through the shelter roof. Particle sampling efficiency was assessed using the particle loss calculator software developed by von der Weiden et al. (2009). The particle transmission was calculated to vary between 99% and 88% for the 0.25–10 μm size range.

2.2.3. Single-Particle Composition

Atmospheric particles were also collected for subsequent analysis by computer-controlled scanning electron microscopy with energy dispersive X-ray spectroscopy (CCSEM-EDX) (Ault et al., 2012). Particle collection was carried out using a 10-stage rotating micro-orifice uniform deposit impactor (MOUDI; model 110-R, MSP Corp.). Ambient air was sampled at a rate of ~22 L min^{-1} through ~1 m of black conductive tubing (3/8") and diluted with an additional ~8 L min^{-1} of particle-free (HEPA-filtered; capsule filter 12,144, Pall Corp.) air for a total flow rate of 30 L min^{-1} into the MOUDI. Particle samples were collected for ~24 hr periods starting at 9:00 local time (AKST). During the ice fog event (29 January 2022–3 February 2022), samples were collected at ~12 hr intervals starting at 9:00 and 21:00 AKST. The MOUDI normally collects particles on rotating stages, which results in a relatively even distribution of particles on the collection substrates (Marple et al., 1991). However, the MOUDI failed to rotate during the entire ice fog event, meaning the particles were not evenly distributed on the substrate. Particles were impacted onto transmission electron microscopy (TEM) grids (Carbon Type-B Formvar film copper grids; Ted Pella, Inc.) on stage 4, with a 50% size cutoff of 1.8–3.2 μm (Marple et al., 1991). After

collection and prior to analysis, samples were stored sealed in the dark at room temperature (approximately 20°C) (Laskina et al., 2015).

CCSEM-EDX analysis of individual particles was conducted using an FEI Quanta environmental SEM operating at 20 kV accelerating voltage, located at the Environmental Molecular Sciences Laboratory at Pacific Northwest National Laboratory. The instrument uses a high angle annular dark field (HAADF) detector for SEM imaging and to determine particle size (projected area and perimeter). An EDX detector (EDAX Inc.) was used to collect elemental composition data for elements larger than Be ($Z > 4$). The relative abundances (mole percent) of the elements C, N, O, Na, Mg, Al, Si, P, S, Cl, K, Ca, Cr, Mn, Fe, Ni, and Zn were quantified for each individual particle. The substrate film and grid contribute to the C, O, and Cu signals, making the measurements of C and O in these particles semiquantitative (Laskin et al., 2006). A summary of the samples analyzed is included in Table S1 of Supporting Information S1. The EDX spectra of 4,247 total individual particles were grouped into 30 clusters based on elemental composition using k-means clustering as described previously (Ault et al., 2012), using code written in MATLAB R2022a (MathWorks Inc.). The clusters were further combined manually into seven different particle classes (dust, fresh road salt, aged road salt, soot, C/O/S (carbon/oxygen/sulfur), *K* (potassium)-rich, and *P* (phosphorus)-rich) based on previous CCSEM-EDX studies (Ault et al., 2012; Axson et al., 2016; Coz et al., 2009; Creamean & Axson et al., 2016; Laskin et al., 2006; Li et al., 2003; McNamara et al., 2020; Pósfai et al., 2003; Sobanska et al., 2014). To study changes in the population of particles during and outside of an ice fog event, samples were grouped into Ice Fog (29 January–3 February) and non-ice fog (26 January–29 January and 4 February–25 February) periods, with the specific dates listed in Table S1 of Supporting Information S1.

2.2.4. Filter Collection for Total Aerosol INP Concentrations

Integrated total aerosol samples were collected for 24 hr (17 January 2022–28 January 2022 and 04 February 2022–21 February 2022) and 12 hr (29 January 2022–03 February 2022) periods throughout ALPACA (see Table S3 in Supporting Information S1). Details of the filters, including their cleaning and filter holders, can be found in several papers, including Creamean and Hill et al. (2022) and Barry, Hill and Jentzsch et al. (2021) and are described briefly here. This system uses a vacuum pump (Thomas oil-less piston compressor /vacuum pump, 2,688 series) that pulls through 47 mm polycarbonate filters (0.2 µm pore size backed with 10-µm polycarbonate filters) at 15 L min^{-1} on average, contained in pre-sterilized, single-use, open face Nalgene™ Sterile Analytical Filter Units. Flow rates are measured continuously in-line using a mass flow meter (TSI 5200-2). The filters are protected under a precipitation shield. The filters were stored frozen at −20°C from collection until analysis 4–15 months later.

2.2.5. Collection of Size-Resolved Samples for Offline INP Analysis

A 4-stage Davis Rotating-drum Unit for Monitoring cascading impactor (DRUM model DA-400; DRUMAir™; Cahill et al., 1987) collected size-resolved aerosol particles. Details on the DRUM can be found in Creamean et al. (2018, 2019), and Creamean and Barry et al. (2022). Briefly, the DRUM collects aerosol particles via impaction on sterilized perfluoroalkoxy substrate strips coated with petrolatum at 4 size ranges from 0.15 to >12 µm in diameter with size cuts at 2.96, 1.21, and 0.34 µm at 27–30 L min^{-1} through a vertical inlet of ∼1 m of 4 cm diameter aluminum tubing. These size ranges cover many aerosols including those that serve as INPs (DeMott et al., 2010). The DRUM impactor was encased in a 47 cm × 35.7 cm × 17.6 cm Pelican™ case. During ALPACA, DRUM samples were collected at a 24 hr temporal resolution from 17 January 2022–28 January 2022 and 05 February 2022–25 February 2022 and 12 hr temporal resolution from 29 January 2022–04 February 2022 (see Table S2 in Supporting Information S1). The DRUM substrates were stored frozen at −20°C from collection until analysis for approximately 13–15 months. The smallest (0.15–0.3 µm) and largest (3–12 µm) size ranges were analyzed from 29 January 2022 21:00–30 January 2022 8:58, 02 February 2022 20:54–03 February 2022 9:04, 18 February 2022 9:00–19 February 2022 8:58, and 24 February 2022 9:58–25 February 2022 8:51. These dates were selected to quantify INP sizes during and outside of the ice fog period.

2.2.6. Processing of INP Samples

Select DRUM substrates and all filter samples were processed on the Colorado State University (CSU) Ice Spectrometer (IS). Details of this process are found in Barry, Hill and Jentzsch et al. (2021) and Creamean and

Hill et al. (2022) but are described briefly here. The filter samples were processed by placing each filter in a 50 mL sterile polypropylene tube with 8 mL of 0.1 µm filtered deionized water and shaken at 200 rpm for 20 min to resuspend particles. The DRUM samples were processed by placing each substrate in a 15 mL sterile polypropylene tube with 5 mL of 0.1 µm filtered deionized water and ultrasonicated for 30s followed by vortexing at 3,200 rpm for seven, 10s pulses. The IS contains two 96-well temperature-controlled aluminum blocks fitted with disposable clean PCR (Polymerase Chain Reaction) trays. Fifty microliter aliquots of the aerosol suspension were dispensed into the PCR trays (within a laminar flow clean hood), the trays were placed in the aluminum blocks in the IS, the blocks were covered with a plexiglass window, and the headspace purged with 750 mL min^{-1} of cooled, dry, particle-free N_2. Frozen aliquots were counted at each 0.5° interval as the temperature was lowered at ~0.33°C min^{-1} to ~−30°C. Eleven-fold dilutions were used to count INPs active at the lowest temperatures. Sample blanks were also collected by briefly exposing them to ambient outdoor conditions but not put in line with the sample flow, then analyzed. INPs in select samples were further characterized through thermal treatments and peroxide digestions to measure the contributions of heat-labile and organic, and inorganic INPs (see Table S3 in Supporting Information S1). To assess the fractional contribution of heat-labile, proteinaceous INPs, the sample was re-tested after heating to 95°C for 20 min (Hill et al., 2016; O'Sullivan et al., 2018; Suski et al., 2018). To remove all organic INPs, 30% H_2O_2 was added to the sample to produce a 10% final concentration then heated to 95°C for 20 min while illuminated with ultraviolet B fluorescent bulbs to generate hydroxyl radicals (residual H_2O_2 was removed using catalase), and the samples were then again processed in the IS (Suski et al., 2018). Remaining INPs are considered inorganic (i.e., likely, though not exclusively, mineral) in nature. In total, 40 filters were processed for total INPs and 8 for heat and peroxide treatments. Significance testing between INP concentrations was performed using a student's *t*-test.

2.2.7. Contextual Meteorological Data

Temperature data were collected via a thermistor epoxied onto 9 mm diameter metal tubes and placed inside polyvinyl chloride radiation shields (Cesler-Maloney et al., 2022). The temperature probe used in this study was deployed at 3 m AGL. The temperature sensor had a precision greater than 0.15°C over 20 to −60°C. Wind speed and direction were measured at 23 m AGL by a wind monitor with propeller and potentiometer. Dew point data were retrieved from Wunderground and collected at Fairbanks International Airport (FAI) (Figure 1).

2.2.8. Levoglucosan Analysis

A subset of the filter extracts were analyzed for levoglucosan. The extracts were analyzed on a Dionex DX-500 series ion chromatograph using high-performance anion-exchange chromatography with pulsed amperometric detection via an ED-50/ED-50A electrochemical cell. This cell has two electrodes: a gold working electrode and a pH-Ag/AgCl (silver/silver chloride) reference electrode. Separation was employed by a sodium hydroxide gradient using a Dionex CarboPac PA-1 column (4 × 250 mm). The run time was 59 min with an injection volume of 100 µL. More details can be found in Sullivan et al. (2019, 2022).

2.2.9. Microphysical Data

Data from a Particle Phase Detector–2000 (PPD2K; Vochezer et al., 2016) was used between 12:00 29 January–9:00 3 February. The PPD2K measures the forward scattered light as particles pass through a laser beam The scattered light can be used to measure particle shape and size. The PPD2K was operated at building 4,070 at Fort Wainwright with its inlet at the ground level (above snowpack). More information can be found in Vas et al. (2021).

3. Results and Discussion

3.1. Ice Fog Event Overview

During the ALPACA study, an ice fog and pollution event occurred from 29 January to 3 February 2022 (Figure 2). The ice fog event was identified through the Fairbanks National Weather Service (NWS) and was further validated by microphysical data (Figure S1 in Supporting Information S1). Outside of the ice fog period daily average temperatures ranged from −24.6°C to 2.0°C and daily average frost point ranged from −21.6°C to 23.1°C. Both were lower during the ice fog/pollution period, where temperature ranged from −20.8°C to −30.4°C and frost point ranged from −29.4°C to −16.9°C. On 31 January, the frost point was greater than the

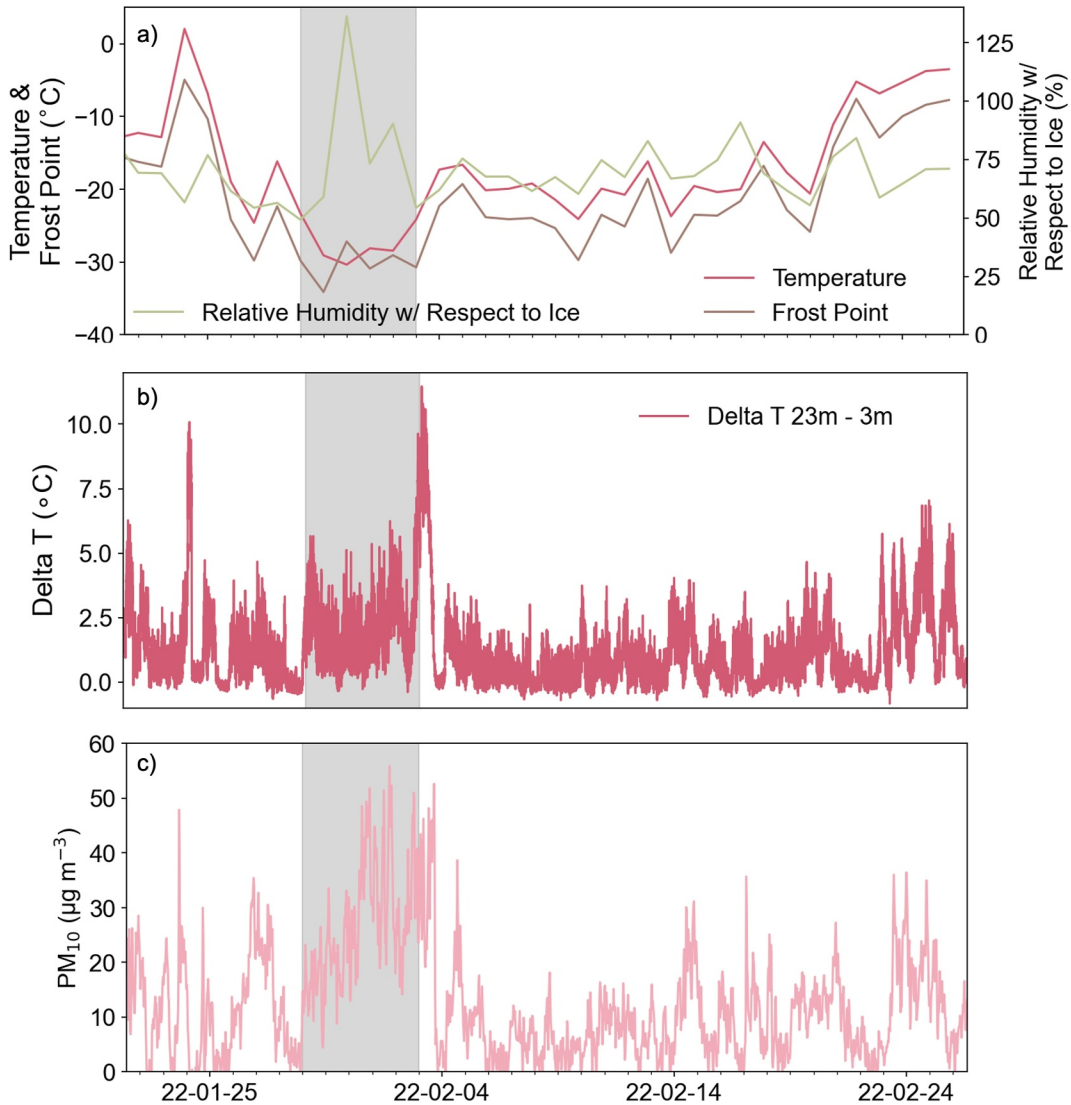

Figure 2. Time series in AKST of (a) daily average meteorological parameters, including air temperature, frost point, and calculated relative humidity with respect to ice (Murphy & Koop, 2005), (b) Inversion strength between 3 and 23 m, and (c) PM_{10} mass concentrations (30 min time resolution) from the downtown Fairbanks site during the 2022 ALPACA campaign. The gray shaded regions highlight the ice fog and pollution event during the campaign.

temperature, indicating a supersaturated environment with respect to ice. It is important to note that on 31 January, since the ambient temperature was below the frost point, that deposition regime nucleation likely occurred while this study only measured immersion mode INPs. Outside of the pollution period, average PM_{10} was 10.6 µg m^{-3} while during the pollution period average PM_{10} was 26.8 µg m^{-3}, which equates to a 150% increase (significant at 95% confidence interval). Winds remained calm (1.0 m s^{-1} on average) during the ice fog period (Figure S2 in Supporting Information S1).

3.2. INP Concentrations

Figure 3 displays the INP concentrations at select temperature ranges and the onset freezing temperature (i.e., the highest temperature in which drops froze and thus INPs were detectable by the CSU IS) from each filter (see complete cumulative (i.e., meaning that any INPs active at −10°C are also active at lower temperatures, etc.) INP spectra in Figure S3 of Supporting Information S1). During the ice fog period, there was no significant change observed for INPs at −25°C; however at −15°C, there was a 58% (significant at 95% confidence interval)

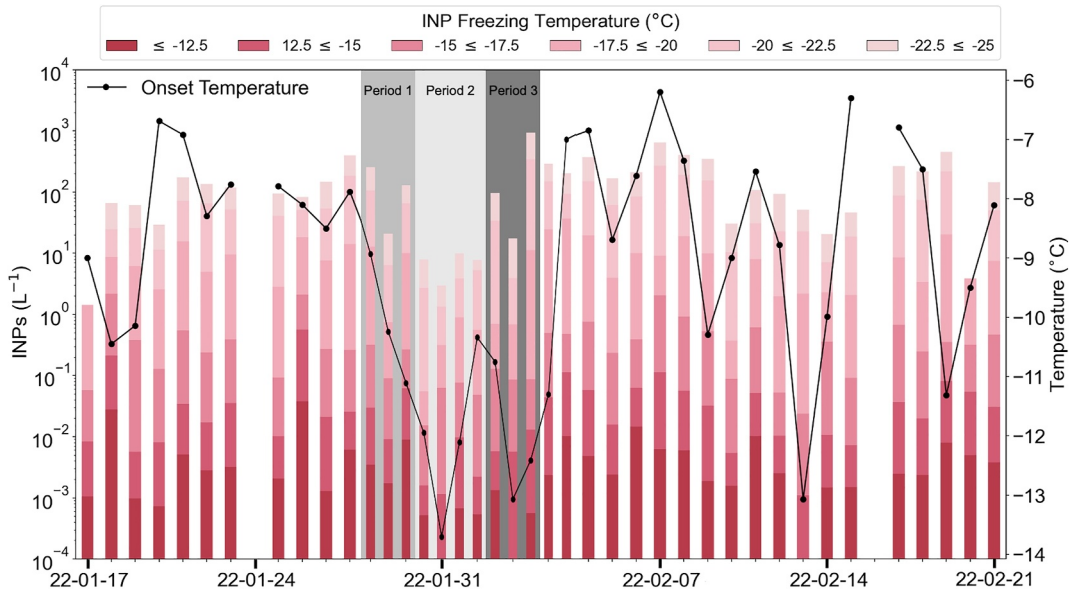

Figure 3. Cumulative ice nucleating particle concentrations per *L* of air at a representative set of freezing temperature values for each total aerosol filter sample collected in downtown Fairbanks at the CTC site. The ice fog period is shaded gray. The wider bars, collected between 17 January–28 January and 4 February–21 February represent the filters collected for a total of 24 hr. The narrow bars, collected between 29 January–4 February, represent filters collected for a total of 12 hr. The first set of bars highlighted in gray represent: (a) Period 1: 29 January 9:00–30 January 21:00 2022, (b) Period 2: 30 January 21:00–1 February 21:00 2022, and (c) Period 3: 1 February 21:00–3 February 9:00 2022. The solid black line shows the onset freezing temperature for each filter.

decrease in INPs. These temperatures were chosen because there were very few INPs detected at −12.5°C and above. The lower INP concentrations during the ice fog period suggest that a subset of the INPs were already activated into fog ice crystals and not captured by the filter unit sampler (i.e., only interstitial INPs were measured), due to the ice fog crystals settling out and the relatively large size of ice fog crystals, which is typically 20–100 μm in diameter (Gultepe et al., 2014). Average INP onset freezing temperatures decreased from −8°C to −11°C during the ice fog period, further suggesting that a majority of INPs with higher onset temperatures had already activated. While ambient temperatures were quite low in the study period of interest, the characterization of INPs at higher temperatures could be critical to understanding ice fog formation, depending on the microphysical pathway taken. Combustion emissions produce water vapor at higher temperatures concurrently with aerosol (e.g., Carrico et al., 2010), which can lead to droplet formation pathways that occur at temperatures well above ambient. Freezing in higher temperature ranges can initiate secondary ice formation processes, increasing the importance of high-temperature INPs (i.e., >−15°C) (Mignani et al., 2019).

During the ice fog period, INPs were still active at −15°C, despite the temperature ranging from −20.8°C to −30.4°C. INPs being active at −15°C despite the temperature being lower during the ice fog period suggests that INP concentrations were not limiting during this event in Fairbanks. The INPs active at −15°C during the ice fog period could be explained by the INPs being from a local source. Jensen et al. (2022) found that a snowstorm in northern Greenland washed out the airborne bacterial community, resulting in low atmospheric concentrations for the next 4 weeks due to a lack of long-range transport and few local sources in the surrounding ice and snow-covered area. This study does not observe such a wash-out for INPs active at −15°C, suggesting that INPs are not likely from long-range transport. A potential local source could be tall vegetation, not covered by snow and ice, which has been shown to produce effective biological INPs (Huang et al., 2021). Another local source of INPs may be residential wood burning. Previous studies have shown that primary biological INPs can originate from biomass burning (Barry, Hill & Levin et al., 2021; Moore et al., 2021). A separate explanation is that the INPs are continually entrained from a source present in warmer air above the inversion (Fridlind et al., 2012).

Within the ice fog period, we defined 3 sub periods: (a) Period 1: 29 January 9:00–30 January 21:00 2022, (b) Period 2: 30 January 21:00–1 February 21:00 2022, and (c) Period 3: 1 February 21:00–3 February 9:00 2022.

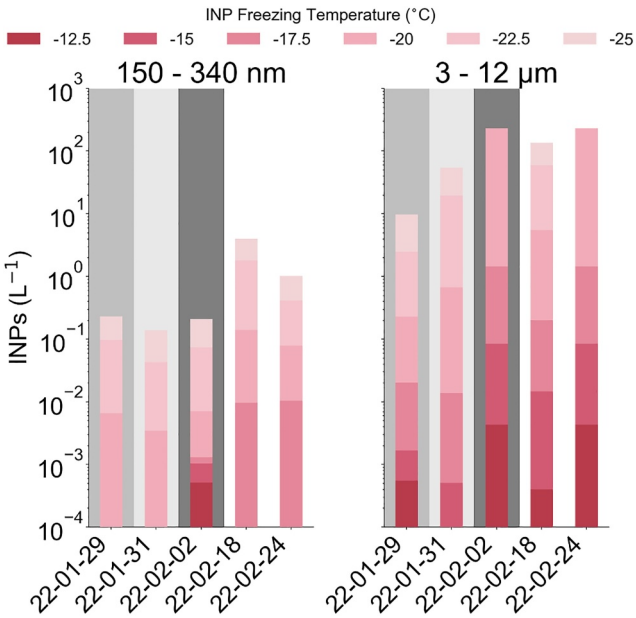

Figure 4. Cumulative ice nucleating particle concentrations at selected temperatures for 3–12 µm and 150–340 nm size bins. Gray shading indicates samples from within the ice fog period.

INP concentrations were generally highest during non-ice fog periods or during period 1 at the warmest freezing temperatures (2×10^{-2} to 9 L^{-1} at ≥ −20°C). Based on the meteorological data, ice fog data, PM_{10}, and INPs, period 1 seemed to be a transitional period between non-ice fog conditions and the peak of the ice fog event during period 2. INP concentrations remained relatively unchanged in period 1 from the non-ice fog period, likely due to the ice fog formation not being limited by available INPs and the less substantial ice fog in the transitional period not effectively scavenging them enough to see a significant decrease. Period 2 was the peak of the pollution event (shown in Figure 2 by the highest PM_{10} concentrations during ALPACA), coincident with the coldest temperatures, highest relative humidity with respect to ice, and highest frost point (Figure 2); highest ice particle concentrations, especially in the 10–20 µm size range (Figure S1 in Supporting Information S1); and most stagnant conditions (Figure S2 in Supporting Information S1). For more information on ice crystal microphysics during the ice fog period, see Schmitt et al. (2024a), Schmitt, Järvinen, et al. (2024). Period 2 also coincided with the lowest INP concentrations of the entire ice fog event (4×10^{-4} to 4 L^{-1} at all freezing temperatures). During period 3, the strongest inversion occurred and wind speed started to pick up from a more northerly direction. PM_{10} remained similar to period 2 (33.7 and 29.9 µg m^{-3}, respectively), while INP concentrations started to increase again, indicating a continued or even new source of INPs that was not as readily scavenged by the thinner ice fog (as demonstrated in Figure S1 of Supporting Information S1), even though winds likely dispersed the existing ice fog particles and pollution aerosol.

Compared to other Arctic and sub-Arctic regions where observations have been collected, Fairbanks had much higher concentrations of INPs during ALPACA. For example, Wex et al. (2019) reported on INP concentrations in multiple Arctic land-based locations and found INP concentrations between 10^{-3}–10^{-2} L^{-1} at −20°C in Alert (Nunavut), Utqiaġvik (Alaska), Ny-Ålesund (Svalbard), and Villum Research Station (Greenland), with the lowest of these values being from the winter months. Creamean et al. (2018) also found INP concentrations between 10^{-3}–10^{-2} L^{-1} at −20°C from March–May at Oliktok Point in Alaska. These values are 1–3 orders of magnitude smaller than the INP concentrations found in Fairbanks at −20°C during ALPACA. The high abundance of INPs in Fairbanks may also be attributed to its inland location. Conen et al. (2023) found that Yakutsk, Russia observed higher INP concentrations (10^{-2}–10^{-1} L^{-1} at −12°C) than coastal Arctic locations (10^{-3}–10^{-2} L^{-1} at −12°C). The lowest INP concentrations in Yakutsk were present in the winter, suggesting that natural sources were responsible for the increased INP concentrations. At −12.5°C in Fairbanks during ALPACA, INP concentrations ranged from 10^{-4}–10° L^{-1}, spanning both smaller and larger in magnitude than the INP concentrations in Conen et al. (2023). Fairbanks is a unique location compared to other sub-Arctic and Arctic regions due to the presence of local urban emission sources. Results from our study align with other studies that might include a mixture of urban and natural sources of aerosol (i.e., they are not densely-populated urban areas like Beijing) (Lacher et al., 2018; Schrod et al., 2020).

3.3. Composition and Size of INPs

Analyses of the 3–12 µm and 150–340 nm particles (340 nm−1.2 and 1.2–3 µm size bins were collected but not analyzed for this study) of the DRUM impactor show that the concentration of INPs in the 3–12 µm size bin is at least two orders of magnitude higher than the 150–340 nm size bin (Figure 4). Figure S4 in Supporting Information S1 shows the complete cumulative INP spectra for these samples. During the autumn and spring of the 2019–2020 Multidisciplinary drifting Observatory for the Study of Arctic Climate (MOSAiC) campaign, super-micron INPs were more abundant, except during the winter Arctic haze when pollution was transported long distances and was present in the central Arctic (Creamean & Barry et al., 2022). Creamean et al. (2018, 2019) also observed more abundant super-micron INPs when the INPs were from a local source (e.g., oilfields and industrial activity). It has also been observed that super-micron INPs are more effective

than sub-micron, when the INPs are composed of mineral dust (Chen et al., 2021; Mason et al., 2016; Reicher et al., 2019).

When evaluating the 3–12 μm and 150–340 nm INPs during the ice fog periods, some unique characteristics manifested. The 3–12 μm INPs were highest during period 3 (although, within the same order of magnitude as non-ice fog periods), supporting the conclusion that there was buildup after the peak ice fog period and potentially a new sources due to the change in winds, ice fog properties, and inversion strength. The 3–12 μm INPs were lowest in concentration during either period 1 or 2 at all freezing temperatures, indicating those were activated at the initiation and peak of the ice fog event. Interestingly, during the ice fog event, 150–340 nm INPs were not present at freezing temperatures $\geq -20°C$ until period 3, corroborating the change in conditions leading to a potentially new source of INPs. However, they were highest during non-ice fog periods and lowest in concentration at freezing temperatures $\leq -17.5°C$ during period 2, indicating they were activated during the peak of the ice fog event and were scavenged following their larger counterparts that started decreasing during period 1. As discussed below, despite the abundance of organic INPs during this study, based on the filter treatments, there was still an inorganic fraction that could have potentially contributed to the large super-micron INP population (e.g., mineral dust). The possible sources of the INPs are discussed in more detail in the following sections that report on aerosol chemical composition.

Figure 5 displays the percent of total INPs that were determined to be inorganic, organic, and/or heat-labile. On average throughout ALPACA, most INPs were heat-labile (63%), followed by organic (31%), with very few INPs being inorganic (6%). Organic INPs peaked during the periods 1 (23%–60%) and 3 (6%–76%) and were lowest during the peak of the ice fog event (period 2) (5%–47%). One scenario consistent with the high percentage of organic INPs overall is that more efficient INPs derived from biological or organic materials, that typically activate at higher freezing temperatures (Testa et al., 2021), may have been depleted by the ice fog and not sampled onto the filter, as daily average temperatures during the ice fog period ranged from $-20.8°C$ to $-30.4°C$. That is, biological INPs are/were activated into the fog before lower temperature INPs such as mineral dust (Koehler et al., 2010). A dominance of organic INPs has been observed in other northern high latitude locations: Barry, Hill and Moore et al. (2023) and Creamean et al. (2020) observed that a majority of INPs in permafrost samples were organic. INPs from biomass burning have been shown to contain large organic fractions (Schill et al., 2020). When biomass burning aerosols dominate the aerosol distribution, organic INPs can be a significant fraction of the total INPs (Barry, Hill & Levin et al., 2021).

Heat-labile INPs were also generally lowest during period 2 (40%–76%), and were highest outside of the ice fog event (54%–97%). However, the relative abundance of heat-labile INPs within and outside the fog period are much more similar to each other than abundances of organic INPs. A potential reason for this could be that the source of the biological INPs is remaining constant both inside and outside the fog period. Such a large biological portion of INPs in Fairbanks during the winter is unexpected due to the extremely low temperatures, but our results from the ALPACA period are consistent with observations in the spring collected over the Prudhoe Bay despite most surfaces being frozen (Creamean et al., 2018). It is also important to note that certain dust types (e.g., quartz dusts, calcite) are sensitive to wet heating unlike common felsic/illitic INPs (Daily et al., 2022). This means there is a possibility that minerals may be reacting to heat treatments, although quartz dusts are minor contributors in most regions. Despite many of the INPs observed in this study being heat-labile or organic, there is still a large fraction of INPs remaining after the treatments that are inorganic during the ice fog period, likely indicating the presence of dust of unknown origin. The dust is potentially from the application of sand and gravel to the roads, leading to road dust, which has been found to be a major source of heat-resistant INPs in the urban atmosphere (Chen et al., 2024).

Inorganic INPs peaked during period 2 (13%–30%), but started to increase during period 1 (0%–3%), and were very low in abundance otherwise. This suggests that (a) there was a source of inorganic INPs during the coldest periods of the ice fog event and/or (b) they were not as efficiently activated during the ice fog event and to some extent remained as interstitial INPs. The former could partially be due to the spreading of gravel on the streets by the city of Fairbanks, which occurs when temperatures become too cold for salt to be effective at deicing, indicating the inorganic INPs could be of mineral nature from mechanical grinding of the gravel to increase friction for vehicles. Also, it has been shown that coal fly ash can serve as an INP, which may be another potential source of inorganic INPs in Fairbanks due to the presence of coal fired power plants (Grawe et al., 2018; Umo et al., 2019). However, fly ash tends to nucleate ice at temperatures below approximately $-30°C$ into the

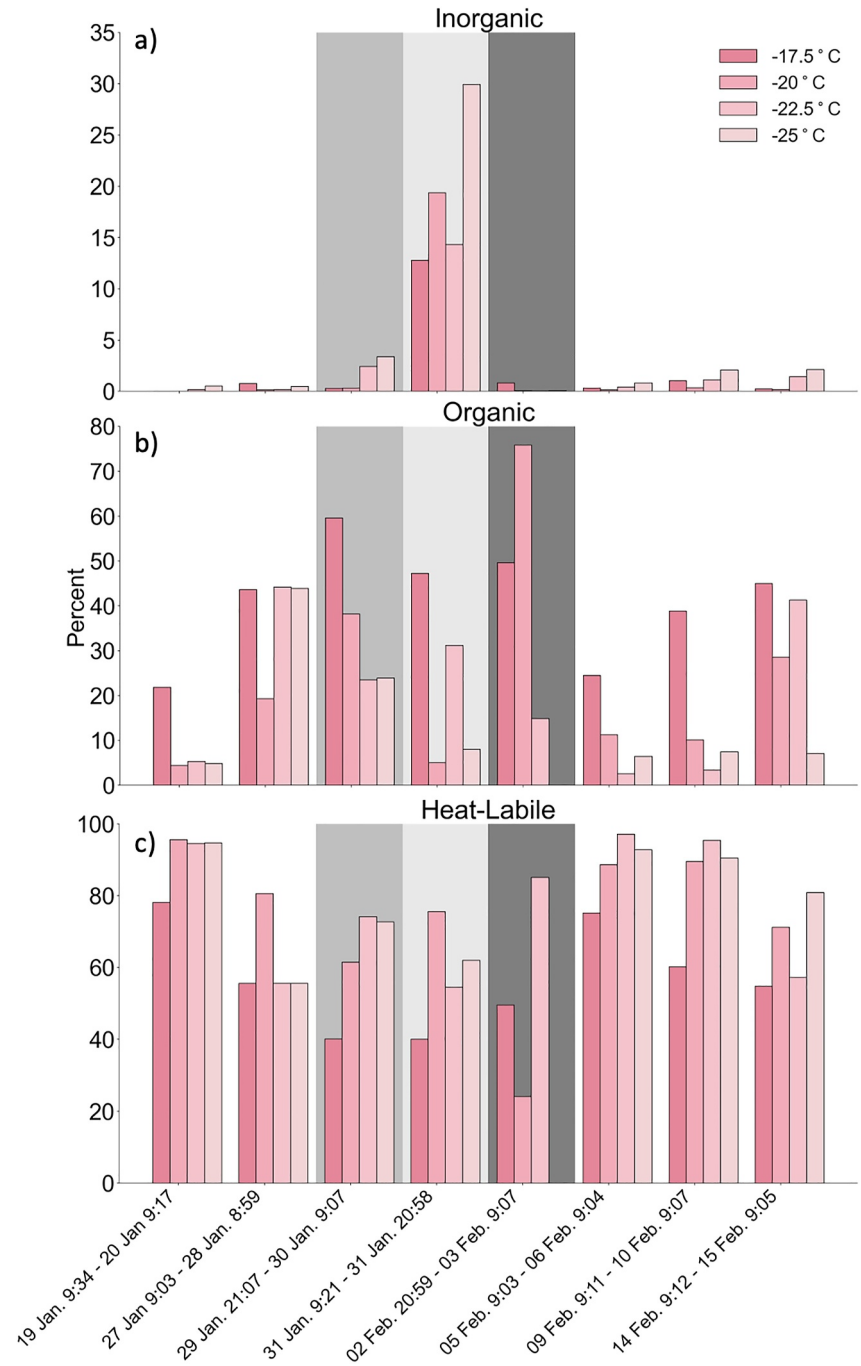

Figure 5. (a) Percent of inorganic ice nucleating particles (INPs), (b) organic (subtraction of INPs remaining after peroxide treatment from INPs remaining after heat treatment) INPs, and (c) heat-labile INPs at selected dates and temperatures. The gray shaded region represents the 3 sub-periods of the ice fog event. Times are presented in AKST.

homogeneous freezing regime, so is likely a minor influence on ice fog formation during ALPACA compared to the heat-labile and organic INPs that are active at much warmer temperatures. Soot has also been shown to be ice nucleation active (e.g., DeMott, 1990; Gao et al., 2022), but some studies have shown it to be inactive under immersion mode ice nucleation (Kanji et al., 2020) or only active at very cold temperatures (e.g., Falk et al., 2021).

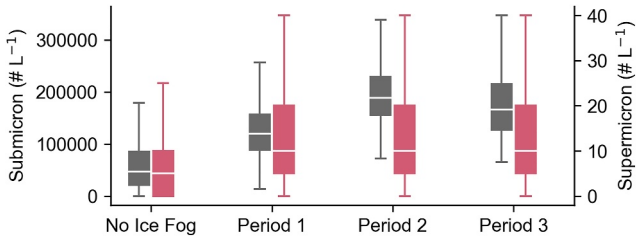

Figure 6. Boxplots of the number concentration (# L^{-1}) of submicron (0.25–1 μm; gray) and supermicron (1–32 μm; pink) aerosol particles for the three ice fog subperiods (Period 1: 29 January 9:00–30 January 21:00 2022, Period 2: 30 January 21:00–1 February 21:00 2022, and Period 3: 1 February 21:00–3 Febuary 9:00 2022) and the non-fog periods. The boxes represent the 25th–75th percentiles, with the median marked by the white lines. The whiskers represent the 5th to 95th percentiles.

3.4. Aerosol Size and Composition

Figure 6 shows aerosol number concentrations for both submicron (0.25–1 μm) and supermicron (1–32 μm) aerosol particles from the non-ice fog and ice fog sub-periods during ALPACA. The submicron aerosol number concentration was 2.8x higher (statistically significant at 95% confidence interval) and less variable toward the peak of the ice fog event in period 2 (2×10^5 L^{-1} on average). Submicron concentration was lowest during non-ice fog periods (6×10^4 L^{-1} on average). This is opposite of the smallest INPs (150–340 nm), which were highest in concentration during non-ice fog periods and lowest during the peak of the ice fog event at freezing temperatures ≤ -20°C (Figure 3). The peak ice fog period also coincided with the peak in PM_{10} and a relatively strong temperature inversion (Figure 2), indicating the pollution was predominantly influenced by submicron aerosol, which might be caused by additional sources from residential combustion during the coldest period being concentrated near the surface from the strong inversion. Even though submicron aerosols tend to be poorer INPs compared to their larger counterparts, a portion of them were still activated into the ice fog due to the cold ambient air temperatures.

The supermicron aerosols had a slightly smaller 2x significant increase in concentration during the ice fog period, and were highest during period 3 (15 L^{-1} on average as opposed to the lowest during non-ice fog periods at 7 L^{-1}). Similar to their smaller counterparts, the 3–12 μm INPs followed an opposite trend from the supermicron aerosol, where they were lowest during periods 1 and 2, and highest during period 3 and non-ice fog periods. Holistically, these results indicate (a) there was additional supermicron aerosol present during the ice fog period, due to either additional sources, concentration near the surface due to the strong inversion, or some combination of the two, and (b) a subset of supermicron aerosols served as effective INPs that started activating at the beginning of the ice fog period and into the peak of the ice fog, until the change in winds and thinning of the ice fog particles during period 3. Overall, the larger INPs were active at warmer temperatures and reached their minima at certain freezing temperatures earlier in the ice fog period than the smaller INPs, even though both sub- and super-micron aerosols increased during the ice fog/pollution event.

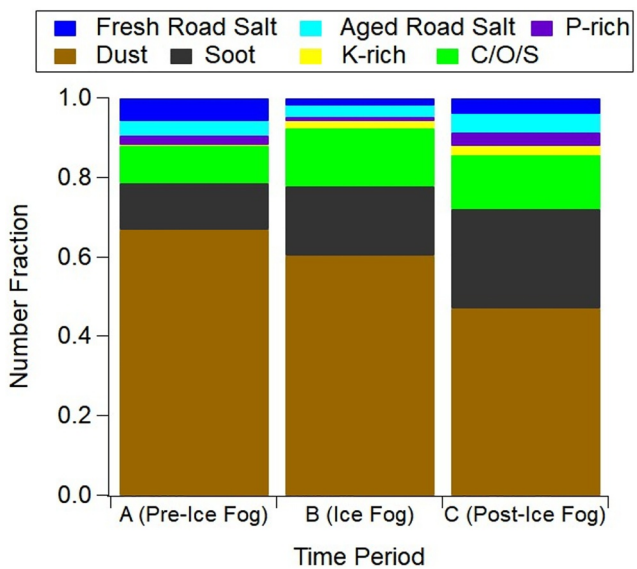

Figure 7. Average number fractions of individual particle types identified by CCSEM-EDX during ice fog (29 January–3 February 2022), and non-ice fog (26–28 January, 2022 and 4–25 February, 2022) conditions. The total number of particles analyzed during ice fog and non-ice fog periods are 783, and 3,464, respectively. See Table S1 in Supporting Information S1 for specific dates and numbers of particles analyzed per sample. All particles were collected on stage 4 (1.8–3.2 μm d_a). P-rich refers to phosphorus-containing particles; K-rich refers to potassium-containing particles, and C/O/S refers to particles composed of carbon, oxygen, and sulfur.

Figure 7 shows the number fraction contributions of the individual particle (1.8–3.2 μm d_a) types, as identified by CCSEM-EDX analysis, for particles collected during ice fog and non-ice fog conditions. Dust was the most abundant particle type, with similar number fractions between the ice fog (44% ± 3%) and non-ice fog (47 ± 2) conditions (Figure 7). These dust particles are consistent with the inorganic INPs that remained as interstitial aerosol during the ice fog period. Dust particles were identified by the presence of Al, Si, Ca, and/or Fe (Axson et al., 2016; Coz et al., 2009; Waza et al., 2023). Soot particles are composed primarily of carbon and have a fractal morphology, indicating their production from combustion sources (Andreae, 1983). The number fraction of soot particles was higher during ice fog (30% ± 1%) compared to during non-ice fog conditions (23% ± 1%) (Figure 7). This is consistent with (a) soot typically being relatively poor INPs and (b) an increase in pollution during the ice fog event. Particles composed of carbon, oxygen, and sulfur (classified as C/O/S) were round and aqueous, suggesting that they were primarily composed of secondary aerosol; these C/O/S particles accounted for similar number fractions during ice fog (19% ± 3%) relative to non-ice fog (19 ± 1%) conditions (Figure 7).

Minor particle types observed included potassium (*K*)-rich particles, likely from biomass and wood combustion (Adachi & Buseck, 2008; Hopkins et al., 2007; Zauscher et al., 2013), phosphorus (*P*)-rich particles from diesel combustion (Karjalainen et al., 2016; Miller et al., 2007; Rodvanna

et al., 2020), and fresh and aged road salt (McNamara et al., 2020). The K-rich number fraction was higher during non-ice fog (2.7% ± 0.2%) relative to ice fog (0.5% ± 0.1%), possibly reflective of (a) local bans on residential wood heating during highly polluted and stagnant conditions and/or (b) biomass burning particles that activated during the ice fog event. The P-rich number fraction was similar during ice fog (1.2% ± 0.7%) as compared to non-ice fog (2.3% ± 0.7%). The number fractions of fresh and aged road salt particles were also similar during ice fog (2.0% ± 0.9% and 3.1% ± 0.9%, respectively) compared to non-ice fog (2.4% ± 0.6% and 4.0% ± 0.6%, respectively).

A strong correlation between levoglucosan and PM_{10} ($R^2 = 0.99$, $n = 6$, Figure S5 in Supporting Information S1), as well as the very high levoglucosan concentrations (ranging from 128–1,190 ng m^{-3}) supports the likelihood that there was a strong residential wood burning influence on the aerosol population, especially during the colder ice fog periods. This correlation may also be in part due to the trapping of pollution due to the strong inversion. Levoglucosan is a commonly used wood burning marker because it is an anhydrosugar produced from the combustion of cellulose (Simoneit et al., 1999). Haque et al. (2021) measured levoglucosan on the top of the International Arctic Research Center (IARC) building at UAF (200 m above sea level) from June 2008–June 2009 and found wintertime concentrations to range from 95.1–214 (mean: 145) ng m^{-3}. Our maximum observed concentration of levoglucosan was 1,190 ng m^{-3}. This order of magnitude difference may be due to the difference in location and ground elevation within the city of Fairbanks (65 m difference). Cesler-Maloney et al. (2022) also shows that $PM_{2.5}$ concentrations were lower aloft than at ground level during strong temperature inversions.

Finally, we used empirical orthogonal function (EOF) analysis to understand variability in PM_{10} metal composition (see Figure S6 in Supporting Information S1). The analysis produced one EOF that explained over 80% of the variance in the PM_{10} metal composition data, and its principal component peaked during ice fog periods 2 and 3. It was composed of sulfur with some potassium, calcium, iron, and zinc, likely indicative of the presence of dust and sulfate aerosol during the ice fog period, as observed by CCSEM-EDX as dust and C/O/S particles (Figure 7). These results are consistent with the single-particle analysis, peak in pollution which can be largely influenced by primary sulfate from combustion sources in Fairbanks (Moon et al., 2024), and presence of interstitial inorganic INPs during the ice fog.

3.5. Potential Sources of INPs in Fairbanks During ALPACA

Based on the composition of the general aerosol population, as well as the composition of the INPs, we are able to infer there are multiple sources of INPs in Fairbanks. Due to the strong correlation between levoglucosan and PM_{10}, there is a distinct wood burning influence on the general aerosol population, which has been shown in previous studies (Wang & Hopke, 2014). INP treatment data shows that there is a substantial presence of organic INPs. The combination of high levoglucosan concentrations and the presence of organic INPs indicate that residential wood burning in Fairbanks is a potential source of INPs. The high percentage of dust particles in the single-particle composition data paired with the increase in inorganic INPs during the ice fog period, and the EOF containing a dust signature indicate that there is additionally a dust source in Fairbanks during ALPACA. Lastly, the high percentage of heat-labile INPs throughout our study indicate that there are highly effective biological INPs present. Both the organic and heat-labile INPs appeared to more readily activate into ice fog crystals as opposed to the inorganic INPs during our observed event. Altogether, we speculate the sources of aerosol particles, particularly that serve as INPs, are from a mixture of road dust (i.e., from gravel laid on the icy roads to increase traction) and residential wood burning. The source of the biological INPs is more challenging to pinpoint and would require further investigation. However, tall vegetation (e.g., black spruce trees) that was not covered by snow and ice, as well as residential wood burning, could potentially contribute to the biological INP population.

4. Conclusions

Here we report on INP concentrations, size, and composition, as well as aerosol composition and size of single particles during and outside of an ice fog event in Fairbanks, Alaska. Potential sources of INPs are summarized in Figure 8. These measurements were a part of the winter 2022 ALPACA campaign with an overarching goal of better understanding atmospheric chemistry under cold and dark conditions.

We observed an ice fog event that occurred from 29 January to 3 February 2022. The ice fog was accompanied by elevated air pollution and low air temperatures. Within the ice fog event, INP concentrations did not change significantly at −25°C but decreased by 58% (significant at 95% confidence interval) at −15°C, indicating that

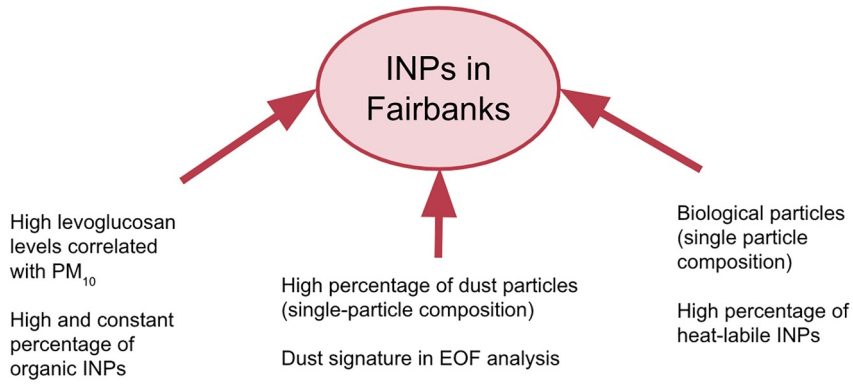

Figure 8. Schematic showing potential ice nucleating particle sources to be (from left to right): residential wood burning, dust, and heat-labile particles.

INPs had likely activated into ice fog crystals, especially INPs active at higher temperatures, and were not captured by the filter units. Overall, most INPs were heat-labile (63%), followed by organic (31%), with very few INPs being inorganic (6%). Organic INPs peaked during periods 1 and 3, heat-labile INPs peaked outside of the ice fog event. Organic and heat-labile INPs were at their lowest concentrations during period 2. Inorganic INPs were low in abundance throughout our study but peaked in concentration during period 2 (13%–30%). Together these results indicate that there was a larger inorganic fraction of INPs inside the ice fog period that were potentially not activated into the ice fog and/or potentially a higher dust concentration during the ice fog period. The fraction of heat-labile INPs decreased during the peak of the ice fog event, indicating they were preferentially activated. Organic and heat-labile INPs dominated the fractional contribution of total INPs, which is consistent with other northern high-latitude locations. Analysis of size-resolved INPs showed a decrease of smaller and larger INPs during the peak of the ice fog event and were highest at most temperatures before (150–340 nm INPs) or during the end (3–12 μm) of the ice fog event due to a change it meteorological conditions affecting the source strength. INPs in the 150–340 nm size range were not observed above −17.5°C until the end of the ice fog event. Aerosol composition measurements indicate the presence of dust, followed by soot and other pollutant aerosol type, while the levoglucosan data indicate an influence from wood burning. Overall, there were quite high INP concentrations in Fairbanks compared to other locations in the Arctic and sub-arctic during winter. These INPs likely facilitated ice fog formation in Fairbanks which has implications for other high latitude locations subject to the hazards associated with ice fog.

Data Availability Statement

The data that support the findings of this study are available from Lill and Creamean (2024), Tenime-roussel and Danna (2024), and Schnaiter et al. (2024).

References

Adachi, K., & Buseck, P. R. (2008). Internally mixed soot, sulfates, and organic matter in aerosol particles from Mexico City. *Atmospheric Chemistry and Physics*, *8*(21), 6469–6481. https://doi.org/10.5194/acp-8-6469-2008

Andreae, M. O. (1983). Soot carbon and excess fine potassium Long-range transport of combustion-derived Aerosols. *Science*, *220*(4602), 1148–1151. https://doi.org/10.1126/science.220.4602.1148

Ault, A. P., Peters, T. M., Sawvel, E. J., Casuccio, G. S., Willis, R. D., Norris, G. A., & Grassian, V. H. (2012). Single-particle SEM-EDX analysis of iron-containing coarse particulate matter in an urban environment: Sources and distribution of iron within Cleveland, Ohio. *Environmental Science & Technology*, *46*(8), 4331–4339. https://doi.org/10.1021/es204006k

Axson, J. L., Shen, H., Bondy, A. L., Landry, C. C., Welz, J., Creamean, J. M., & Ault, A. P. (2016). Transported mineral dust deposition case study at a hydrologically sensitive mountain site: Size and composition shifts in ambient aerosol and snowpack. *Aerosol and Air Quality Research*, *16*(3), 555–567. https://doi.org/10.4209/aaqr.2015.05.0346

Barry, K. R., Hill, T. C. J., Jentzsch, C., Moffett, B. F., Stratmann, F., & DeMott, P. J. (2021a). Pragmatic protocols for working cleanly when measuring ice nucleating particles. *Atmospheric Research*, *250*, 105419. https://doi.org/10.1016/j.atmosres.2020.105419

Barry, K. R., Hill, T. C. J., Levin, E. J. T., Twohy, C. H., Moore, K. A., Weller, Z. D., et al. (2021b). Observations of ice nucleating particles in the free troposphere from Western US wildfires. *Journal of Geophysical Research: Atmospheres*, *126*(3), e2020JD033752. https://doi.org/10.1029/2020JD033752

Barry, K. R., Hill, T. C. J., Moore, K. A., Douglas, T. A., Kreidenweis, S. M., DeMott, P. J., & Creamean, J. M. (2023a). Persistence and potential atmospheric ramifications of ice-nucleating particles released from thawing permafrost. *Environmental Science & Technology*, *57*(9), 3505–3515. https://doi.org/10.1021/acs.est.2c06530

Acknowledgments
We thank Martin Schnaiter (Karlsruhe Institute of Technology) and Emma Jaervinen (Karlsruhe Institute of Technology) for their work in providing the microphysical data. Swarup China (PNNL EMSL) is thanked for facilitation of the CCSEM-EDX measurements. We thank the University of Alaska-Fairbanks for field campaign logistical support. B. D'A., K.S.L and B.T.-M. acknowledge support from the Agence National de Recherche (ANR) CASPA (Climate-relevant Aerosol Sources and Processes in the Arctic) project (Grant ANR-21-CE01-0017), and the Institut polaire français Paul-Émile Victor (IPEV) (Grant 1215) and CNRS-INSU programme LEFE (Les Enveloppes Fluides et l'Environnement) ALPACA-France projects. We acknowledge support from the National Science Foundation AGS-2037119, AGS-2037091, and RISE-1927831. CCSEM-EDX data collection was performed at the Environmental Molecular Sciences Laboratory (EMSL), a national science user facility sponsored by the U.S. Department of Energy Office of Biological and Environmental Research located at the Pacific Northwest National Laboratory (PNNL). Travel funds to PNNL were provided in part by the University of Michigan Rackham Graduate School.

Barry, K. R., Hill, T. C. J., Nieto-Caballero, M., Douglas, T. A., Kreidenweis, S. M., DeMott, P. J., & Creamean, J. M. (2023b). Active thermokarst regions contain rich sources of ice-nucleating particles. *Atmospheric Chemistry and Physics*, *23*(24), 15783–15793. https://doi.org/10.5194/acp-23-15783-2023

Benson, C. S. (1970). Ice fog. *Weather*, *25*(1), 11–18. https://doi.org/10.1002/j.1477-8696.1970.tb03223.x

Bi, K., McMeeking, G. R., Ding, D. P., Levin, E. J. T., DeMott, P. J., Zhao, D. L., et al. (2019). Measurements of ice nucleating particles in Beijing, China. *Journal of Geophysical Research (Atmospheres)*, *124*(14), 8065–8075. https://doi.org/10.1029/2019JD030609

Borys, R. D. (1989). Studies of ice nucleation by Arctic aerosol on AGASP-II. *Journal of Atmospheric Chemistry*, *9*(1), 169–185. https://doi.org/10.1007/BF00052831

Bowling, S. A. (1986). Climatology of high-latitude air pollution as illustrated by Fairbanks and anchorage, Alaska. *Journal of Climate and Applied Meteorology*, *25*(1), 22–34. https://doi.org/10.1175/1520-0450(1986)025<0022:cohlap>2.0.co;2

Burkart, J., Steiner, G., Reischl, G., Moshammer, H., Neuberger, M., & Hitzenberger, R. (2010). Characterizing the performance of two optical particle counters (Grimm OPC1.108 and OPC1.109) under urban aerosol conditions. *Journal of Aerosol Science*, *41*(10), 953–962. https://doi.org/10.1016/j.jaerosci.2010.07.007

Cahill, T. A., Feeney, P. J., & Eldred, R. A. (1987). Size-time composition profile of aerosols using the drum sampler. *Nuclear Instruments and Methods in Physics Research Section B: Beam Interactions with Materials and Atoms*, *22*(1), 344–348. https://doi.org/10.1016/0168-583X(87)90355-7

Carrico, C. M., Petters, M. D., Kreidenweis, S. M., Sullivan, A. P., McMeeking, G. R., Levin, E. J. T., et al. (2010). Water uptake and chemical composition of fresh aerosols generated in open burning of biomass. *Atmospheric Chemistry and Physics*, *10*(11), 5165–5178. https://doi.org/10.5194/acp-10-5165-2010

Cesler-Maloney, M., Simpson, W. R., Miles, T., Mao, J., Law, K. S., & Roberts, T. J. (2022). Differences in ozone and particulate matter between ground level and 20 m aloft are frequent during wintertime surface-based temperature inversions in Fairbanks, Alaska. *Journal of Geophysical Research: Atmospheres*, *127*(10), e2021JD036215. https://doi.org/10.1029/2021JD036215

Chen, J., Wu, Z., Augustin-Bauditz, S., Grawe, S., Hartmann, M., Pei, X., et al. (2018). Ice-nucleating particle concentrations unaffected by urban air pollution in Beijing, China. *Atmospheric Chemistry and Physics*, *18*(5), 3523–3539. https://doi.org/10.5194/acp-18-3523-2018

Chen, J., Wu, Z., Chen, J., Reicher, N., Fang, X., Rudich, Y., & Hu, M. (2021). Size-resolved atmospheric ice-nucleating particles during East Asian dust events. *Atmospheric Chemistry and Physics*, *21*(5), 3491–3506. https://doi.org/10.5194/acp-21-3491-2021

Chen, J., Wu, Z., Gong, X., Qiu, Y., Chen, S., Zeng, L., & Hu, M. (2024). Anthropogenic dust as a significant source of ice-nucleating particles in the urban environment. *Earth's Future*, *12*(1), e2023EF003738. https://doi.org/10.1029/2023EF003738

Conen, F., Morris, C. E., Leifeld, J., Yakutin, M. V., & Alewell, C. (2011). Biological residues define the ice nucleation properties of soil dust. *Atmospheric Chemistry and Physics*, *11*(18), 9643–9648. https://doi.org/10.5194/acp-11-9643-2011

Conen, F., Yakutin, M. V., Puchnin, A. N., & Yttri, K. E. (2023). On coarse patterns in the atmospheric concentration of ice nucleating particles. *Atmospheric Research*, *285*, 106645. https://doi.org/10.1016/j.atmosres.2023.106645

Coz, E., Gómez-Moreno, F. J., Pujadas, M., Casuccio, G. S., Lersch, T. L., & Artíñano, B. (2009). Individual particle characteristics of North African dust under different long-range transport scenarios. *Atmospheric Environment*, *43*(11), 1850–1863. https://doi.org/10.1016/j.atmosenv.2008.12.045

Creamean, J. M., Axson, J. L., Bondy, A. L., Craig, R. L., May, N. W., Shen, H., et al. (2016a). Changes in precipitating snow chemistry with location and elevation in the California Sierra Nevada. *Journal of Geophysical Research: Atmospheres*, *121*(12), 7296–7309. https://doi.org/10.1002/2015JD024700

Creamean, J. M., Neiman, P. J., Coleman, T., Senff, C. J., Kirgis, G., Alvarez, R. J., & Yamamoto, A. (2016b). Colorado air quality impacted by long-range-transported aerosol: A set of case studies during the 2015 Pacific Northwest fires. *Atmospheric Chemistry and Physics*, *16*(18), 12329–12345. https://doi.org/10.5194/acp-16-12329-2016

Creamean, J. M., Kirpes, R. M., Pratt, K. A., Spada, N. J., Maahn, M., de Boer, G., et al. (2018). Marine and terrestrial influences on ice nucleating particles during continuous springtime measurements in an Arctic oilfield location. *Atmospheric Chemistry and Physics*, *18*(24), 18023–18042. https://doi.org/10.5194/acp-18-18023-2018

Creamean, J. M., Mignani, C., Bukowiecki, N., & Conen, F. (2019). Using freezing spectra characteristics to identify ice-nucleating particle populations during the winter in the Alps. *Atmospheric Chemistry and Physics*, *19*(12), 8123–8140. https://doi.org/10.5194/acp-19-8123-2019

Creamean, J. M., Hill, T. C. J., DeMott, P. J., Uetake, J., Kreidenweis, S., & Douglas, T. A. (2020). Thawing permafrost: An overlooked source of seeds for Arctic cloud formation. *Environmental Research Letters*, *15*(8), 084022. https://doi.org/10.1088/1748-9326/ab87d3

Creamean, J. M., Barry, K., Hill, T. C. J., Hume, C., DeMott, P. J., Shupe, M. D., et al. (2022a). Annual cycle observations of aerosols capable of ice formation in central Arctic clouds. *Nature Communications*, *13*(1), 3537. https://doi.org/10.1038/s41467-022-31182-x

Creamean, J. M., Hill, T. C. J., & Hume, C. (2022b). Ice Nucleation Spectrometer (INS) instrument handbook. https://doi.org/10.2172/1846263

Daily, M. I., Tarn, M. D., Whale, T. F., & Murray, B. J. (2022). An evaluation of the heat test for the ice-nucleating ability of minerals and biological material. *Atmospheric Measurement Techniques*, *15*(8), 2635–2665. https://doi.org/10.5194/amt-15-2635-2022

David, R. O., Marcolli, C., Fahrni, J., Qiu, Y., Perez Sirkin, Y. A., Molinero, V., et al. (2019). Pore condensation and freezing is responsible for ice formation below water saturation for porous particles. *Proceedings of the National Academy of Sciences*, *116*(17), 8184–8189. https://doi.org/10.1073/pnas.1813647116

DeMott, P. J., Prenni, A. J., Liu, X., Kreidenweis, S. M., Petters, M. D., Twohy, C. H., et al. (2010). Predicting global atmospheric ice nuclei distributions and their impacts on climate. *Proceedings of the National Academy of Sciences*, *107*(25), 11217–11222. https://doi.org/10.1073/pnas.0910818107

DeMott, P. J., Mason, R. H., McCluskey, C. S., Hill, T. C. J., Perkins, R. J., Desyaterik, Y., et al. (2018). Ice nucleation by particles containing long-chain fatty acids of relevance to freezing by sea spray aerosols. *Environmental Science: Processes and Impacts*, *20*(11), 1559–1569. https://doi.org/10.1039/C8EM00386F

DeMott, P. J. (1990). An exploratory study of ice nucleation by soot aerosols. *Journal of Applied Meteorology and Climatology*, *29*(10), 1072–1079. https://doi.org/10.1175/1520-0450(1990)0292.0.CO;2

Falk, J., Korhonen, K., Malmborg, V. B., Gren, L., Eriksson, A. C., Karjalainen, P., et al. (2021). Immersion freezing ability of freshly emitted soot with various physico-chemical characteristics. *Atmosphere*, *12*(9), 1173. https://doi.org/10.3390/atmos12091173

Fridlind, A. M., van Diedenhoven, B., Ackerman, A. S., Avramov, A., Mrowiec, A., Morrison, H., et al. (2012). A FIRE-ACE/SHEBA case study of mixed-phase arctic boundary layer clouds: Entrainment rate limitations on rapid primary ice nucleation processes. *Journal of the Atmospheric Sciences*, *69*, 365–389. https://doi.org/10.1175/JAS-D-11-052.1

Gao, K., Zhou, C.-W., Meier, E. J. B., & Kanji, Z. A. (2022). Laboratory studies of ice nucleation onto bare and internally mixed soot–sulfuric acid particles. *Atmospheric Chemistry and Physics*, *22*(8), 5331–5364. https://doi.org/10.5194/acp-22-5331-2022

Grawe, S., Augustin-Bauditz, S., Clemen, H.-C., Ebert, M., Eriksen Hammer, S., Lubitz, J., et al. (2018). Coal fly ash: Linking immersion freezing behavior and physicochemical particle properties. *Atmospheric Chemistry and Physics*, *18*(19), 13903–13923. https://doi.org/10.5194/acp-18-13903-2018

Gultepe, I., Kuhn, T., Pavolonis, M., Calvert, C., Gurka, J., Heymsfield, A. J., et al. (2014). Ice fog in arctic during FRAM–ice fog project: Aviation and nowcasting applications. *Bulletin of the American Meteorological Society*, *95*(2), 211–226. https://doi.org/10.1175/BAMS-D-11-00071.1

Gultepe, I., Heymsfield, A., Gallagher, M., Ickes, L., & Baumgardner, D. (2017). Ice fog: The current state of knowledge and future challenges. *American Meteorological Society: Meteorological Monographs*, *58*, 4.1–4.24. https://doi.org/10.1175/AMSMONOGRAPHS-D-17-0002.1

Haque, M. M., Kawamura, K., Deshmukh, D. K., Kunwar, B., & Kim, Y. (2021). Biomass burning is an important source of organic aerosols in interior Alaska. *Journal of Geophysical Research: Atmospheres*, *126*(12), e2021JD034586. https://doi.org/10.1029/2021JD034586

Heim, M., Mullins, B. J., Umhauer, H., & Kasper, G. (2008). Performance evaluation of three optical particle counters with an efficient "multimodal" calibration method. *Journal of Aerosol Science*, *39*(12), 1019–1031. https://doi.org/10.1016/j.jaerosci.2008.07.006

Hill, T. C. J., DeMott, P. J., Tobo, Y., Fröhlich-Nowoisky, J., Moffett, B. F., Franc, G. D., & Kreidenweis, S. M. (2016). Sources of organic ice nucleating particles in soils. *Atmospheric Chemistry and Physics*, *16*(11), 7195–7211. https://doi.org/10.5194/acp-16-7195-2016

Hoose, C., & Möhler, O. (2012). Heterogeneous ice nucleation on atmospheric aerosols: A review of results from laboratory experiments. *Atmospheric Chemistry and Physics*, *12*(20), 9817–9854. https://doi.org/10.5194/acp-12-9817-2012

Hopkins, R. J., Lewis, K., Desyaterik, Y., Wang, Z., Tivanski, A. V., Arnott, W. P., et al. (2007). Correlations between optical, chemical and physical properties of biomass burn aerosols. *Geophysical Research Letters*, *34*(18), L18806. https://doi.org/10.1029/2007GL030502

Huang, S., Hu, W., Chen, J., Wu, Z., Zhang, D., & Fu, P. (2021). Overview of biological ice nucleating particles in the atmosphere. *Environment International*, *146*, 106197. https://doi.org/10.1016/j.envint.2020.106197

Huffman, P. J., & Ohtake, T. (1971). Formation and growth of ice fog particles at Fairbanks, Alaska. *Journal of Geophysical Research (1896–1977)*, *76*(3), 657–665. https://doi.org/10.1029/JC076i003p00657

Jensen, L. Z., Glasius, M., Gryning, S.-E., Massling, A., Finster, K., & Šantl-Temkiv, T. (2022). Seasonal variation of the atmospheric bacterial community in the Greenlandic high arctic is influenced by weather events and local and distant sources. *Frontiers in Microbiology*, *13*, 909980. https://doi.org/10.3389/fmicb.2022.909980

Joyce, P. L., von Glasow, R., & Simpson, W. R. (2014). The fate of NO_x emissions due to nocturnal oxidation at high latitudes: 1-D simulations and sensitivity experiments. *Atmospheric Chemistry and Physics*, *14*(14), 7601–7616. https://doi.org/10.5194/acp-14-7601-2014

Kanji, Z. A., Ladino, L. A., Wex, H., Boose, Y., Burkert-Kohn, M., Cziczo, D. J., & Krämer, M. (2017). Overview of ice nucleating particles. *Meteorological Monographs*, *58*(1), 1.1–1.33. https://doi.org/10.1175/AMSMONOGRAPHS-D-16-0006.1

Kanji, Z. A., Welti, A., Corbin, J. C., & Mensah, A. A. (2020). Black carbon particles do not matter for immersion mode ice nucleation. *Geophysical Research Letters*, *47*(11), e2019GL086764. https://doi.org/10.1029/2019GL086764

Karjalainen, P., Ntziachristos, L., Murtonen, T., Wihersaari, H., Simonen, P., Mylläri, F., et al. (2016). Heavy duty diesel exhaust particles during engine motoring formed by lube oil consumption. *Environmental Science & Technology*, *50*(22), 12504–12511. https://doi.org/10.1021/acs.est.6b03284

Kikuchi, K. (1971a). Observation of cloud condensation Nuclei at Syowa station, Antarctica. *Journal of the Meteorological Society of Japan. Ser. II*, *49*(5), 376–383. https://doi.org/10.2151/jmsj1965.49.5_376

Kikuchi, K. (1971b). Observations of concentration of Ice Nuclei at Syowa Station, Antarctica. *Journal of the Meteorological Society of Japan. Ser. II*, *49*(1), 20–31. https://doi.org/10.2151/jmsj1965.49.1_20

Kikuchi, K. (1972). Sintering phenomenon of frozen cloud particles observed at Syowa station, Antarctica. *Journal of the Meteorological Society of Japan. Ser. II*, *50*(2), 131–135. https://doi.org/10.2151/jmsj1965.50.2_131

Koehler, K. A., Kreidenweis, S. M., DeMott, P. J., Petters, M. D., Prenni, A. J., & Möhler, O. (2010). Laboratory investigations of the impact of mineral dust aerosol on cold cloud formation. *Atmospheric Chemistry and Physics*, *10*(23), 11955–11968. https://doi.org/10.5194/acp-10-11955-2010

Kramshøj, M., Vedel-Petersen, I., Schollert, M., Rinnan, Å., Nymand, J., Ro-Poulsen, H., & Rinnan, R. (2016). Large increases in Arctic biogenic volatile emissions are a direct effect of warming. *Nature Geoscience*, *9*(5), 349–352. https://doi.org/10.1038/ngeo2692

Kumai, M. (1964). A study of ice fog and Ice-Fog nuclei at Fairbanks, Alaska, Part I. In *This digital resource was created from scans of the print resource [report]*. Cold Regions Research and Engineering Laboratory (U.S.). Retrieved from https://erdc-library.erdc.dren.mil /jspui/handle/11681/5757

Kumai, M. (1966). Electron microscopic study of ice-fog and ice-crystal Nuclei in Alaska. *Journal of the Meteorological Society of Japan. Ser. II*, *44*(3), 185–194. https://doi.org/10.2151/jmsj1965.44.3_185

Lacher, L., Steinbacher, M., Bukowiecki, N., Herrmann, E., Zipori, A., & Kanji, Z. A. (2018). Impact of air mass conditions and aerosol properties on ice nucleating particle concentrations at the high altitude research station Jungfraujoch. *Atmosphere*, *9*(9), 363. https://doi.org/10.3390/atmos9090363

Larsen, J. N., & Fondahl, G. (2015). *Arctic human development report: Regional processes and global linkages*. Nordisk Ministerråd. Retrieved from https://urn.kb.se/resolve?urn=urn:nbn:se:norden:org:diva-3809

Laskin, A., Cowin, J. P., & Iedema, M. J. (2006). Analysis of individual environmental particles using modern methods of electron microscopy and X-ray microanalysis. *Journal of Electron Spectroscopy and Related Phenomena*, *150*(2), 260–274. https://doi.org/10.1016/j.elspec.2005.06.008

Laskina, O., Morris, H. S., Grandquist, J. R., Estillore, A. D., Stone, E. A., Grassian, V. H., & Tivanski, A. V. (2015). Substrate-deposited sea spray aerosol particles: Influence of analytical method, substrate, and storage conditions on particle size, phase, and morphology. *Environmental Science & Technology*, *49*(22), 13447–13453. https://doi.org/10.1021/acs.est.5b02732

Law, K. S., & Stohl, A. (2007). Arctic air pollution: Origins and impacts. *Science (New York, N.Y.)*, *315*(5818), 1537–1540. https://doi.org/10.1126/science.1137695

Law, K. S., Stohl, A., Quinn, P. K., Brock, C. A., Burkhart, J. F., Paris, J.-D., et al. (2014). Arctic air pollution: New insights from POLARCAT-IPY. *Bulletin of the American Meteorological Society*, *95*(12), 1873–1895. https://doi.org/10.1175/BAMS-D-13-00017.1

Law, K. S., Roiger, A., Thomas, J. L., Marelle, L., Raut, J.-C., Dalsøren, S., et al. (2017). Local Arctic air pollution: Sources and impacts. *Ambio*, *46*(3), 453–463. https://doi.org/10.1007/s13280-017-0962-2

Levin, E. J. T., DeMott, P. J., Suski, K. J., Boose, Y., Hill, T. C. J., McCluskey, C. S., et al. (2019). Characteristics of Ice Nucleating Particles in and Around California Winter Storms. *Journal of Geophysical Research: Atmospheres*, *124*(21), 11530–11551. https://doi.org/10.1029/2019JD030831

Li, J., Pósfai, M., Hobbs, P. V., & Buseck, P. R. (2003). Individual aerosol particles from biomass burning in Southern Africa: 2, Compositions and aging of inorganic particles. *Journal of Geophysical Research*, *108*(D13), 8484. https://doi.org/10.1029/2002JD002310

Li, C., Hsu, N. C., Sayer, A. M., Krotkov, N. A., Fu, J. S., Lamsal, L. N., et al. (2016). Satellite observation of pollutant emissions from gas flaring activities near the Arctic. *Atmospheric Environment*, *133*, 1–11. https://doi.org/10.1016/j.atmosenv.2016.03.019

Lill, E., & Creamean, J. (2024). Ice-Nucleating Particle (INP) and Particulate Matter 10 (PM10) metal concentrations in Fairbanks, Alaska during the Alaskan Layered Pollution And Chemical Analysis (ALPACA)-2022 field study. https://doi.org/10.18739/A2Z892H0K

Malingowski, J., Atkinson, D., Fochesatto, J., Cherry, J., & Stevens, E. (2014). An observational study of radiation temperature inversions in Fairbanks, Alaska. *Polar Science*, *8*(1), 24–39. https://doi.org/10.1016/j.polar.2014.01.002

Marple, V. A., Rubow, K. L., & Behm, S. M. (1991). A Microorifice Uniform Deposit Impactor (MOUDI): Description, calibration, and use. *Aerosol Science and Technology*, *14*(4), 434–446. https://doi.org/10.1080/02786829108959504

Mason, R. H., Si, M., Chou, C., Irish, V. E., Dickie, R., Elizondo, P., et al. (2016). Size-resolved measurements of ice-nucleating particles at six locations in North America and one in Europe. *Atmospheric Chemistry and Physics*, *16*(3), 1637–1651. https://doi.org/10.5194/acp-16-1637-2016

McNamara, S. M., Kolesar, K. R., Wang, S., Kirpes, R. M., May, N. W., Gunsch, M. J., et al. (2020). Observation of road salt aerosol driving Inland wintertime atmospheric chlorine chemistry. *ACS Central Science*, *6*(5), 684–694. https://doi.org/10.1021/acscentsci.9b00994

Mignani, C., Creamean, J. M., Zimmermann, L., Alewell, C., & Conen, F. (2019). New type of evidence for secondary ice formation at around −15 °C in mixed-phase clouds. *Atmospheric Chemistry and Physics*, *19*(2), 877–886. https://doi.org/10.5194/acp-19-877-2019

Miller, A. L., Stipe, C. B., Habjan, M. C., & Ahlstrand, G. G. (2007). Role of lubrication oil in particulate emissions from a hydrogen-powered internal combustion engine. *Environmental Science & Technology*, *41*(19), 6828–6835. https://doi.org/10.1021/es070999r

Moon, A., Jongebloed, U., Dingilian, K. K., Schauer, A. J., Chan, Y.-C., Cesler-Maloney, M., et al. (2024). Primary sulfate is the dominant source of particulate sulfate during winter in Fairbanks, Alaska. *ACS ES&T Air*, *1*(3), 139–149. https://doi.org/10.1021/acsestair.3c00023

Moore, R. A., Bomar, C., Kobziar, L. N., & Christner, B. C. (2021). Wildland fire as an atmospheric source of viable microbial aerosols and biological ice nucleating particles. *The ISME Journal*, *15*(2), 461–472. https://doi.org/10.1038/s41396-020-00788-8

Murphy, D. M., & Koop, T. (2005). Review of the Vapour pressures of ice and supercooled water for atmospheric applications. *Quarterly Journal of the Royal Meteorological Society*, *131*(608), 1539–1565. https://doi.org/10.1256/qj.04.94

Murray, B. J., O'Sullivan, D., Atkinson, J. D., & Webb, M. E. (2012). Ice nucleation by particles immersed in supercooled cloud droplets. *Chemical Society Reviews*, *41*(19), 6519–6554. https://doi.org/10.1039/C2CS35200A

Nicholls, D. L., Brackley, A. M., & Barber, V. (2010). *Wood energy for residential heating in Alaska: Current conditions, attitudes, and expected use. Gen. Tech. Rep. PNW-GTR-826* (Vol. 30). U.S. Department of Agriculture, Forest Service, Pacific Northwest Research Station. 826. https://doi.org/10.2737/PNW-GTR-826

O'Sullivan, D., Adams, M. P., Tarn, M. D., Harrison, A. D., Vergara-Temprado, J., Porter, G. C. E., et al. (2018). Contributions of biogenic material to the atmospheric ice-nucleating particle population in North Western Europe. *Scientific Reports*, *8*(1), 13821. https://doi.org/10.1038/s41598-018-31981-7

Petters, M. D., Parsons, M. T., Prenni, A. J., DeMott, P. J., Kreidenweis, S. M., Carrico, C. M., et al. (2009). Ice nuclei emissions from biomass burning. *Journal of Geophysical Research*, *114*(D7), D07209. https://doi.org/10.1029/2008JD011532

Pósfai, M., Simonics, R., Li, J., Hobbs, P. V., & Buseck, P. R. (2003). Individual aerosol particles from biomass burning in Southern Africa: 1. Compositions and size distributions of carbonaceous particles. *Journal of Geophysical Research*, *108*(D13), 8483. https://doi.org/10.1029/2002JD002291

Radke, L. F., Hobbs, P. V., & Pinnons, J. E. (1976). Observations of CloudCondensation Nuclei, sodium-containing particles, ice nuclei and the light-scattering coefficient near Barrow, Alaska. *Journal of Applied Meteorology*, *15*(9), 982–995. https://doi.org/10.1175/1520-0450(1976)015<0982:ooccns>2.0.co;2

Reicher, N., Budke, C., Eickhoff, L., Raveh-Rubin, S., Kaplan-Ashiri, I., Koop, T., & Rudich, Y. (2019). Size-dependent ice nucleation by airborne particles during dust events in the Eastern Mediterranean. *Atmospheric Chemistry and Physics*, *19*(17), 11143–11158. https://doi.org/10.5194/acp-19-11143-2019

Robinson, E., Thuman, W. C., & Wiggins, E. J. (1957). Ice fog as a problem of air pollution in the Arctic. *Arctic*, *10*(2), 88–104. https://doi.org/10.14430/arctic3756

Rodvanna, S., Srilomsak, M., Shinshi, M., & Hanamura, K. (2020). Scanning electron microscopic time-lapse visualization of Ash movement during regeneration of diesel particulate filters. *International Journal of Automotive Engineering*, *11*(2), 14–21. https://doi.org/10.20485/jsaeijae.11.2_14

Schill, G. P., DeMott, P. J., Emerson, E. W., Rauker, A. M. C., Kodros, J. K., Suski, K. J., et al. (2020). The contribution of black carbon to global ice nucleating particle concentrations relevant to mixed-phase clouds. *Proceedings of the National Academy of Sciences*, *117*(37), 22705–22711. https://doi.org/10.1073/pnas.2001674117

Schmale, J., Arnold, S. R., Law, K. S., Thorp, T., Anenberg, S., Simpson, W. R., et al. (2018). Local Arctic air pollution: A neglected but serious problem *Earth's Future*, *6*(10), 1385–1412. https://doi.org/10.1029/2018EF000952

Schmitt, C. G., Stuefer, M., Heymsfield, A. J., & Kim, C. K. (2013). The microphysical properties of ice fog measured in urban environments of Interior Alaska. *Journal of Geophysical Research: Atmospheres*, *118*(19), 11136–11147. https://doi.org/10.1002/jgrd.50822

Schmitt, C. G., Järvinen, E., Schnaiter, M., Vas, D., Hartl, L., Wong, T., & Stuefer, M. (2024). Classification of ice particle shapes using machine learning on forward light scattering images. *Artificial Intelligence for the Earth Systems*. https://doi.org/10.1175/AIES-D-23-0091.1

Schmitt, C. G., Vas, D., Schnaiter, M., Järvinen, E., Hartl, L., Wong, T., et al. (2024). Microphysical characterization of boundary layer ice particles: Results from a 3-year measurement campaign in interior Alaska. https://doi.org/10.1175/JAMC-D-23-0190.1

Schnaiter, M., Järvinen, E., & Schmitt, C. G. (2024). PPD-2K ice fog particle size and shape distributions from ALPACA (p. 2,6 MB). https://doi.org/10.35097/1935

Schrod, J., Thomson, E. S., Weber, D., Kossmann, J., Pöhlker, C., Saturno, J., et al. (2020). Long-term deposition and condensation ice-nucleating particle measurements from four stations across the globe. *Atmospheric Chemistry and Physics*, *20*(24), 15983–16006. https://doi.org/10.5194/acp-20-15983-2020

Simoneit, B. R. T., Schauer, J. J., Nolte, C. G., Oros, D. R., Elias, V. O., Fraser, M. P., et al. (1999). Levoglucosan, a tracer for cellulose in biomass burning and atmospheric particles. *Atmospheric Environment*, *33*(2), 173–182. https://doi.org/10.1016/S1352-2310(98)00145-9

Simpson, I. J., Akagi, S. K., Barletta, B., Blake, N. J., Choi, Y., Diskin, G. S., et al. (2011). Boreal forest fire emissions in fresh Canadian smoke plumes: C_1-C_{10} volatile organic compounds (VOCs), CO_2, CO, NO_2, NO, HCN and CH_3CN. *Atmospheric Chemistry and Physics*, *11*(13), 6445–6463. https://doi.org/10.5194/acp-11-6445-2011

Simpson, W., Law, K., Schmale, J., Pratt, K., Arnold, S., Mao, J., et al. (2019). Alaskan Layered Pollution And Chemical Analysis (ALPACA) white paper.

Simpson, W. R., Mao, J., Fochesatto, G. J., Law, K. S., DeCarlo, P. F., Schmale, J., et al. (2024). Overview of the Alaskan Layered Pollution And Chemical Analysis (ALPACA) field experiment. *ACS ES&T Air*, *1*(3), 200–222. https://doi.org/10.1021/acsestair.3c00076

Sobanska, S., Falgayrac, G., Rinetz-Planchon, J., Perdrix, E., Brémard, C., & Barbillat, J. (2014). Resolving the internal structure of individual atmospheric aerosol particle by the combination of Atomic Force Microscopy, ESEM–EDX, Raman and ToF–SIMS imaging. *Microchemical Journal*, *114*, 89–98. https://doi.org/10.1016/j.microc.2013.12.007

Sullivan, A. P., Guo, H., Schroder, J. C., Campuzano-Jost, P., Jimenez, J. L., Campos, T., et al. (2019). Biomass burning markers and residential burning in the WINTER aircraft campaign. *Journal of Geophysical Research: Atmospheres*, *124*(3), 1846–1861. https://doi.org/10.1029/2017JD028153

Sullivan, A. P., Pokhrel, R. P., Shen, Y., Murphy, S. M., Toohey, D. W., Campos, T., et al. (2022). Examination of brown carbon absorption from wildfires in the western US during the WE-CAN study. *Atmospheric Chemistry and Physics*, *22*(20), 13389–13406. https://doi.org/10.5194/acp-22-13389-2022

Suski, K. J., Hill, T. C. J., Levin, E. J. T., Miller, A., DeMott, P. J., & Kreidenweis, S. M. (2018). Agricultural harvesting emissions of ice-nucleating particles. *Atmospheric Chemistry and Physics*, *18*(18), 13755–13771. https://doi.org/10.5194/acp-18-13755-2018

Tenine-roussel, B., & Danna, B. (2024). Particle number concentration measured at Fairbanks, Alaska, the Alpaca campaign (local time period: 2022/01/17 08:50 to 2022/02/26 09:51). https://doi.org/10.18739/A2TH8BP6T

Testa, B., Hill, T. C. J., Marsden, N. A., Barry, K. R., Hume, C. C., Bian, Q., et al. (2021). Ice nucleating particle connections to regional Argentinian land surface emissions and weather during the cloud, aerosol, and complex terrain interactions experiment. *Journal of Geophysical Research: Atmospheres*, *126*(23), e2021JD035186. https://doi.org/10.1029/2021JD035186

Tian, P., Liu, D., Bi, K., Huang, M., Wu, Y., Hu, K., et al. (2022). Evidence for Anthropogenic organic aerosols contributing to ice nucleation. *Geophysical Research Letters*, *49*(17), e2022GL099990. https://doi.org/10.1029/2022GL099990

Tran, H. N. Q., & Mölders, N. (2011). Investigations on meteorological conditions for elevated PM2.5 in Fairbanks, Alaska. *Atmospheric Research*, *99*(1), 39–49. https://doi.org/10.1016/j.atmosres.2010.08.028

Umo, N. S., Wagner, R., Ullrich, R., Kiselev, A., Saathoff, H., Weidler, P. G., et al. (2019). Enhanced ice nucleation activity of coal fly ash aerosol particles initiated by ice-filled pores. *Atmospheric Chemistry and Physics*, *19*(13), 8783–8800. https://doi.org/10.5194/acp-19-8783-2019

Vas, D. A., Peckham, S. E., Schmitt, C. G., Stuefer, M., Burgener, R. G., & Wong, T. E. (2021). Ice fog monitoring near Fairbanks, AK. [Report]. Cold Regions Research and Engineering Laboratory (U.S.). Retrieved from https://erdc-library.erdc.dren.mil /jspui/handle/11681/40019

Vochezer, P., Järvinen, E., Wagner, R., Kupiszewski, P., Leisner, T., & Schnaiter, M. (2016). In situ characterization of mixed phase clouds using the Small Ice Detector and the Particle Phase Discriminator. *Atmospheric Measurement Techniques*, *9*(1), 159–177. https://doi.org/10.5194/amt-9-159-2016

von der Weiden, S.-L., Drewnick, F., & Borrmann, S. (2009). Particle loss calculator–A new software tool for the assessment of the performance of aerosol inlet systems. *Atmospheric Measurement Techniques*, *2*(2), 479–494. https://doi.org/10.5194/amt-2-479-2009

Wang, Y., & Hopke, P. K. (2014). Is Alaska truly the great escape from Air pollution? Long term source apportionment of fine particulate matter in Fairbanks, Alaska. *Aerosol and Air Quality Research*, *14*(7), 1875–1882. https://doi.org/10.4209/aaqr.2014.03.0047

Waza, A., Schneiders, K., Heuser, J., & Kandler, K. (2023). Analysis of size distribution, chemical composition, and optical properties of mineral dust particles from dry deposition measurement in Tenerife: Determined by single-particle characterization. *Atmosphere*, *14*(4), 700. https://doi.org/10.3390/atmos14040700

Wendler, G., & Jayaweera, K. O. L. F. (1972). Some measurements of the development of the surface inversion in Central Alaska during winter. *Pure and Applied Geophysics*, *99*(1), 209–221. https://doi.org/10.1007/BF00875277

Wex, H., Huang, L., Zhang, W., Hung, H., Traversi, R., Becagli, S., et al. (2019). Annual variability of ice-nucleating particle concentrations at different Arctic locations. *Atmospheric Chemistry and Physics*, *19*(7), 5293–5311. https://doi.org/10.5194/acp-19-5293-2019

Willis, R. A., & Grice, G. K. (1977). The wintertime Arctic front and its effect on Fairbanks, Alaska. *Monthly Weather Review*, *105*(1), 78–85. https://doi.org/10.1175/1520-0493(1977)105<0078:TWAFAI>2.0.CO;2

Woo, S. H. L., Liu, J. C., Yue, X., Mickley, L. J., & Bell, M. L. (2020). Air pollution from wildfires and human health vulnerability in Alaskan communities under climate change. *Environmental Research Letters*, *15*(9), 094019. https://doi.org/10.1088/1748-9326/ab9270

Zauscher, M. D., Wang, Y., Moore, M. J. K., Gaston, C. J., & Prather, K. A. (2013). Air quality impact and physicochemical aging of biomass burning aerosols during the 2007 San Diego wildfires. *Environmental Science & Technology*, *47*(14), 7633–7643. https://doi.org/10.1021/es4004137

Zhang, C., Wu, Z., Chen, J., Chen, J., Tang, L., Zhu, W., et al. (2022). Ice-nucleating particles from multiple aerosol sources in the urban environment of Beijing under mixed-phase cloud conditions. *Atmospheric Chemistry and Physics*, *22*(11), 7539–7556. https://doi.org/10.5194/acp-22-7539-2022

Zhao, B., Wang, Y., Gu, Y., Liou, K.-N., Jiang, J. H., Fan, J., et al. (2019). Ice nucleation by aerosols from anthropogenic pollution. *Nature Geoscience*, *12*(8), 602–607. https://doi.org/10.1038/s41561-019-0389-4